Too Close, Yet Too Far: Common Envelope Interaction of Triple Systems

By

Adam Batten

A thesis submitted to Macquarie University

for the degree of Master of Research

Department of Physics and Astronomy

January 2018

MACQUARIE
University
SYDNEY·AUSTRALIA

Typeset in LaTeX 2_ε.

Except where acknowledged in the customary manner, the
material presented in this thesis is, to the best of my knowl-
edge, original and has not been submitted in whole or part
for a degree in any university.

Adam Batten

Acknowledgements

First and foremost, I need to give a big thank you to my supervisor Orsola de Marco. Without her wonderful support and guidance in this project everything beyond this page would not be possible.

Also a huge thank you to Jan Staff and Roberto Iaconi. Jan performed the original simulations for this project and was a vital contact, his feedback and suggestions on my project was very helpful. Roberto was a huge help in every aspect of the data analysis, often spending his time teaching me how to run my own simulations for which I am very grateful.

To my house mate Alice, who has lived though my incessant onslaught of puns of varying quality. Our late night rants and rambling therapy sessions has probably helped to keep me as sane as I probably could wish to be when writing a thesis.

Next I have to thank my friend Missy for: (1) scientifically proving that she is able to make me laugh from anywhere in the world via Skype, (2) being the sole person responsible for my quokka knowledge and photo collection increasing by 10,000%. Most importantly (3) being one of my closest friends whilst simultaneously being one of the farthest from me.

To my fellow masters students Arv, Bron, Bryte, Connor, Matt, Oliver, Stephen and Tash. Our lunches were often the highlights of my day and not solely because I got to eat food and avoid doing work. Also shout out to my physics buddies Alastair, Caro, Tim and Tom for surviving undergrad with me. Special mention to Tom for being the best rubber duck debugger I've ever had. For times when a rubber duck simply wont cut it, thanks to James and Wilfred for helping find those bugs in my code.

Finally, and the most importantly, I have to thank my Dad, my Mum and my brother Luke. Without them, I would not be the person who I am today. My Dad instilled a sense of curiosity in me from a young age, encouraging me to ask questions about the world. Whether the answers he gave were true or were made up on the spot is still up for debate.

Abstract

The common envelope interaction is a short lived phase in the evolution of binary systems. A number of evolved binary systems have been discovered that have separations too large to fit our understanding of the common envelope, and yet they are too close that a common envelope interaction must have occurred. In some of these systems, an outer tertiary companion is present, suggesting that the presence of an additional companion could have an influence on the final separation of the inner binary. We present the first hydrodynamic simulations of common envelope interactions involving triple systems. The first simulation contains a low-mass giant with two planets, the second is a 10 $M_\odot$ RGB star with two solar-mass companions. We observe in our simulations that the outermost companion tends to move outward (or at best remains at a similar distance) from its initial position. Our findings do not support the hypothesis that a triple system could provide a pathway to leave the outer companion at an intermediate separation after a common envelope interaction.

Contents

1

Introduction

A binary system consists of two stars in orbit around each other, bound together by their mutual gravitational force. Binary systems are of a great interest in astronomy as the majority of stars with mass larger than the Sun do not exist on their own, but have one or more companions.

Almost all O-type stars on the main sequence are in multiple stellar systems, with $\sim 71\%$ expected to interact with their companion at some point in their lifetime (Sana et al., 2012). The binary fraction for spectral classes B through F is approximately $60 - 50\%$ (Kouwenhoven et al., 2005; Fuhrmann & Chini, 2012; Duchêne & Kraus, 2013; Fuhrmann & Chini, 2015), for G- and K-types its $46 - 42\%$ (Raghavan et al., 2010), and for M-types down to brown dwarfs is $26 - 22\%$ (Duchêne & Kraus, 2013).

If the stars in a binary system are sufficiently close together, when one of the stars evolves off the main sequence and begins to expand, the growing star can interact with its companion by transferring mass onto it. Under certain circumstances, stable mass transfer can become unstable and gives rise to a "common envelope" (CE) event.

In this chapter we will introduce the CE interaction, outlining its importance and explaining the physics involved. We will also present observations of typical post-CE binaries. We will then present observations of binaries that orbit each other close enough that they must have gone through a CE phase, yet they are unlike regular post-CE binaries. Lastly we will suggest how a triple system may affect the CE and play a role in the formation of these systems.

1.1   The importance of the CE interaction

The CE interaction is a phase in the evolution of a binary system where one of the stars expands rapidly to many times its original size, engulfing its companion(s) or planetary system, causing two or more stars to orbit inside a single shared envelope. Orbital in-spiral of the companion(s) results in a close binary and an ejected envelope or in a merger.

As reviewed by Ivanova et al. (2013), the CE phase is the cornerstone of our understanding of many important astrophysical phenomena, because it is likely to be the main pathway to form most evolved, compact binaries including those containing white dwarfs (WD), neutron stars (NS) or black holes (BH). These binaries are the progenitors of type Ia supernovae (SNe Ia), gamma ray bursts and can be sources of detectable gravitational waves. The CE is also responsible for the formation of X-ray binaries, cataclysmic variables and at least one in five planetary nebulae (PNe). For a review how stellar evolution is affected by companions see De Marco & Izzard (2017).

Despite its importance in astrophysics, the CE phase is still poorly understood. The CE interaction is a complex problem that involves numerous physical processes and a huge range of space and time scales, making it difficult to model both analytically and computationally.

1.1.1   Cataclysmic variables and other compact binaries

Paczynski (1976) put forth the CE interaction to explain the formation of V 471 Tau, a pre-cataclysmic variable (a main sequence star and a WD in a close binary) with an orbital separation much smaller than the radius of the WD progenitor. Since the WD progenitor was, in the past, larger than the orbit is today, the binary must have had a much larger separation in the past. The CE phase is currently the favoured mechanism to dramatically reduce the orbital separation in such binary systems.

There are many other classes of compact evolved, binaries whose formation is best explained by a CE interaction. They include low- and high-mass X-ray binaries (a NS or BH accreting from a low- or high-mass star), cataclysmic variables (a WD accreting from a main sequence star) and all combinations of close, double degenerate binaries. The CE interaction can also lead to the companion merging with the core of the primary, which has been hypothesised to explain a range of transient events including V838 Mon (Bond et al., 2003), V 1309 Sco (Tylenda et al., 2011), NGC 4490-OT (Smith et al., 2016), M101-OT (Blagorodnova et al., 2017) and M31-2015 LRN (Macleod et al., 2017b). The merger of a NS with a giant inside a CE is also hypothesised to form exotic objects known as Thorne-Żytkow objects where a NS merges with a red supergiant becoming the supergiants core (Thorne & Żytkow, 1977)).

1.1.2 Type Ia supernovae and gravitational waves

SNe Ia are energetic outbursts presenting no hydrogen in their spectra. They are currently modelled as the thermonuclear explosion of a carbon-oxygen WD that reached the Chandrasaker limit because of accretion from a companion or because of the merger of two WDs (Hillebrandt & Niemeyer, 2000).

SNe Ia are incredibly important as both standardiseable candles used to measure the rate of expansion of the Universe (Riess et al., 1998) and as tools to understand the star formation histories of galaxies (Hopkins & Beacom, 2006). Binary population synthesis models are used to calculate the rate of SNe Ia events. By comparing calculated to observed rates we can determine the likely progenitor of SNe Ia (Livio & Pringle, 2011). However, uncertainties in the CE interaction carry through to uncertainties in the population synthesis models, resulting in large uncertainties in estimates of the SNe Ia outburst rate (Claeys et al., 2014; Toonen et al., 2014). These uncertainties are one of the main stumbling blocks preventing models from identifying the progenitors of SNe Ia.

One of main unknowns is the efficiency at which the orbital energy is transferred to the envelope. As a result we cannot predict the post-CE orbital separation(s), and this translates directly into our ignorance of the time it takes a post-CE binary to explode as a SN Ia. This is further complicated when considering that double degenerate systems such as binary NSs have likely experienced multiple CE phases (Belczyński & Kalogera, 2001).

Gravitational wave astronomy also requires binary population synthesis models to predict the expected number of binary BH and NS merger events. With the first four gravitational wave detections from the Advanced Laser Interferometer and Gravitational-Wave Observatory (Advanced LIGO) being from merger of binary BHs (Abbott et al., 2016a,b, 2017a,b), and with the most recent detection being from a binary NS merger (Abbott et al., 2017c), a huge amount of new information on binary systems will soon be available. However, for the data to be interpreted we require a far better grasp on CE theory in massive binaries.

1.1.3 The morphologies of planetary nebulae

PNe are expanding shells of luminous gas that have been ejected from low- and intermediate-mass stars during the end phase of their evolution. Observations from the Hubble Space Telescope indicate that PNe show a range of different morphologies (approximately 20% are spherical with the remaining 80% showing deviation from spherical symmetry (Jones & Boffin, 2017)).

Traditionally PN shaping has been explained with a combination of a fast-rotating star, with or without a global magnetic field leading to increased mass-loss at the equator Garcia-Segura et al. (1999).

Occasionally, the direct interaction with a closely-orbiting companion may have also been involved in the shaping of the PN. However, there is currently no theory to explain how a single star can have the required rotational velocity (García-Segura et al., 2014) and or global magnetic fields cannot be sustained in a single mass-losing giant (Soker, 2006; Nordhaus et al., 2007). This leaves a binary interaction as the only known mechanism to explain extreme shapes, where the companion could be the agent promoting the magnetic fields and the rotation or could shape the outflow directly (De Marco, 2009). Currently, we don't know the PN binary fraction but we do know that at least one in five PN form via a CE interaction, because we can detect the post-CE binary (Jones & Boffin, 2017). The PN around these binaries are therefore ejected CEs.

1.2   The physics of the CE interaction

Stars in binary systems can evolve differently than they would in isolation, since they are influenced by the gravitational potential of their companions (Taam & Sandquist, 2000). In regions close to each star, the gravitational potential is dominated by that star. However, farther away from the stellar surface, the gravity of the companion plays a role and causes an elongation of the gravitational potential. This restricts the material gravitationally bound to each star in a binary to a tear-shaped volume known as the Roche lobe. Material outside of the Roche lobe can fall onto the companion, orbit around both stars or escape from the system entirely. The size of a star's Roche lobe is typically measured by an average radius R_{RL}, defined such that $4/3\pi R_{RL}^3$ has the same volume as the Roche lobe (Eggleton, 1983):

$$R_{RL} = a \times \frac{0.49\ q^{2/3}}{0.6\ q^{2/3} + \ln\left(1 + q^{1/3}\right)}, \tag{1.1}$$

where a and q are the orbital separation of the system and the mass ratio between the primary and the companion respectively. In this work we will be using 'primary' to refer to the donor star (i.e $q = M_1/M_2$).

Evolved stars such as red giant branch (RGB) or asymptotic giant branch (AGB) stars grow to hundreds of times the size of their progenitors. As described by Paczynski (1976), if a giant star has a companion sufficiently close, its radius growth will be limited and the star will expand to fill its Roche lobe. As the star continues to expand, mass is transferred onto the companion through the first Lagrangian point (L_1 in Fig. 1.1), this is known as Roche lobe overflow (RLOF). Once both the primary star and its companion have filled their Roche lobes, the system enters the CE phase, and the companion is rapidly engulfed by the primary. The CE dynamical phase is very short: a typical time scale for the CE interaction is of the order of the dynamical time scale of the star, which, for solar-mass giants, is between a month and a year depending on its radius.
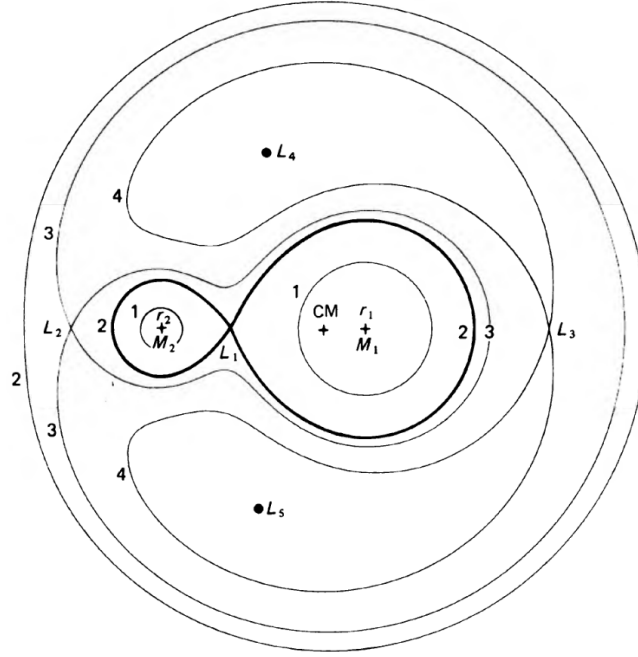
Figure 1.1: The equipotential surfaces around an orbiting binary system. The Roche lobes of the two stars are shown here by the thick black line. M_1 and M_2 are the masses of the primary and the companion, respectively. When M_1 fills its Roche lobe it will transfer mass onto M_2 through the inner Lagrangian point, L_1. Adapted from (Iben & Livio, 1993).

Once the companion starts to in-spiral inside the giant's envelope it creates a wake of material behind it as it moves through the medium. The gravitational interaction between the companion and this wake creates a drag force, causing the companion to slow down and in-spiral towards the core of the primary. We call this drag "gravitational drag" to distinguish it from hydrodynamic drag which tends to be much weaker. Iben & Livio (1993) approximated the gravitational drag, F_{drag}, on the engulfed companion to be:

$$F_{\mathrm{drag}} = \xi \pi R_a^2 \rho \, (v - v_e)^2 \;, \tag{1.2}$$

where ρ is the local density, $v - v_e$ is the relative velocity between the companion (v) and the envelope gas (v_e), ξ is a factor that depends on Mach number (see also Ostriker (1999)), and R_a is the accretion radius which is given by:

$$R_a = \frac{2GM}{(v - v_e)^2 + c_s^2} \;, \tag{1.3}$$

where G is the gravitational constant, M is the mass of the companion and c_s is the sound speed[1]. Using 3D hydrodynamic simulations of wind tunnels, Macleod & Ramirez-Ruiz (2015) and Macleod et al. (2017a) found that density gradients across the direction of motion also affect the strength of the gravitational drag, but this has not been captured by any analytical formalisms so far.

As the companion in-spirals towards the centre of the primary, its orbital energy is dissipated into the envelope. The gas around the companion is both accelerated and heated due to the formation of weak

---

[1]This formulation is for subsonic speeds.

shocks. If enough orbital energy is transferred into the envelope, the envelope can be ejected from the system. Alternatively, if the envelope doesn't have the required energy to escape the companion, it will presumably merge with the core of the primary.

The standard "energy formalism" description of the CE interaction equates the binding energy of the envelope (the energy required to unbind the gas in the envelope) to the difference in orbital energy between the initial and final configurations (van den Heuvel, 1976; Webbink, 1984, 2008). There are many forms of the energy formalism in the literature (De Marco et al., 2011), however the most common form of the energy formalism is shown in Eq. (1.4) (de Kool, 1990; Dewi & Tauris, 2000; Ivanova et al., 2013):

$$ -\frac{GM_1 M_{1,\text{env}}}{\lambda R_1} = -\alpha_{\text{CE}} \left(\frac{GM_1 M_2}{2a_i} - \frac{GM_{1,c} M_2}{2a_f} \right) . \tag{1.4} $$

Here a_i and a_f are the initial and final binary separations respectively, M_1 and M_2 are the masses of the primary and the companion at the time of CE, $M_{1,c}$ is the final mass of the primary after losing its envelope, $M_{1,\text{env}}$ and R_1 are the envelope mass and radius of the primary at the onset of RLOF, λ is a parameter that depends on the structure of the star. Dewi & Tauris (2000) find λ ranges between 0.2 and 0.8 for main sequence stars, but it can be much higher ($\lambda > 5$) for low mass AGB (De Marco et al., 2011)). Finally, α_{CE} is the CE efficiency parameter which describes the fraction of available orbital energy that is used in ejecting the envelope.

By assuming a value for α_{CE}, a value for the final separation(s) can be derived for a binary system containing a CE interaction making reasonable assumptions. What simulations have shown, however, is that there is no single value of α_{CE} and that orbital energy *never* succeeds in unbinding the envelope, even if the binding energy is low and the orbital in-spiral is large (Iaconi et al., 2017a).

This description is common in the literature, but this formalism neglects the effects recombination energy (Nandez et al., 2015; Nandez & Ivanova, 2016; Ivanova & Nandez, 2016), which is likely of importance in determining whether the CE interaction will lead to envelope ejection or a merger event (see Section 2.2).

1.3   Too close, yet too far

Post-CE binaries typically comprise one or two evolved stars at an orbital separation of a few solar radii. There is however observational evidence of a diverse group of evolved binary and triple systems, whose orbital separation is quite a bit larger than typical post CE systems, yet small enough that a CE must have taken place. These systems include post-AGB binaries, a triple system comprising a pulsar and two WDs, and a circumbinary planetary system.

1.3.1   Post AGB binaries

A class of post-AGB stars were discovered to have circumbinary disks encircling a binary with an orbital period between 100 and 2000 days (Van Winckel, 2003; Van Winckel et al., 2009). Presumably, those of these binaries with the shortest periods must have gone through a CE at some point in their history, because their orbit is smaller than the primary's progenitor size. Yet, this CE did not lead to the dramatic in-spiral typical of post-CE binaries, which are typically observed to have periods of hours to a day. Hence these binaries are *too close* together to have avoided a CE interaction, but they are *too far* from each other to fit our understanding of a CE in-spiral.

1.3.2   A millisecond pulsar in a triple system

A pulsar is a highly magnetised, rotating NS with collimated beams of electromagnetic radiation emitted from its poles, likely formed after a massive star undergoes a supernova explosion. The rotational period of a pulsar is extremely regular, ranging from milliseconds to a few seconds.

The millisecond pulsar PSR J0337+1715, discovered by Ransom et al. (2014), is unusual in that it is a NS (mass of 1.438 $M_\odot$) with *two* WD companions (with masses of 0.197 $M_\odot$ and 0.410 $M_\odot$). This system is highly hierarchical, with a tight inner binary (period 1.63 days) and an outer companion at a much farther distance (period 327 days).

Tauris & van den Heuvel (2014) proposed that this system could have formed in a CE event followed by two low-mass X-ray binary phases. The CE scenario proposed involves a 9.9 $M_\odot$ RGB primary entering a CE with a 1.1 $M_\odot$ main sequence companion. A second, outer, 1.3 $M_\odot$ main sequence companion should have orbited farther out from the binary with a period of 4020 days. The model proposed by Tauris & van den Heuvel (2014) suggests that both the companion stars must have suffered some in-spiral during the CE phase, indicating that the outer companion must be close enough to be affected by the gas being ejected by the interaction of the inner companion and the giant, but far enough to have avoided the full force of the CE event.

1.3.3   Surviving planets

Planets are regularly found around main sequence stars in short-period orbits (e.g., Udry & Santos, 2007). However, planets with short-period orbits have also been found around evolved stars, whose precursor had a radius larger than that of the planets' orbit today (Charpinet et al., 2011). Hence the planet must have experienced a CE with the giant progenitor of its host star at some point in the past and survived. Since we can observe these planets, these observations suggest that planets are not

destined to merge with the core of their host star, but are able to survive the CE interaction, although this does not appear likely from the energetic point of view (Staff et al., 2016b; Passy et al., 2012a). Staff et al. (2016b) found in their simulations that even massive planets are unable to survive a CE interaction, and they instead merge with the core.

NN Serpentis (NN Ser) is a post-CE eclipsing binary system consisting of WD and a red dwarf (Parsons et al., 2010). A circumbinary planetary system has been detected around this binary, consisting of two planets (Beuermann et al., 2010; Marsh et al., 2013) with orbital periods of approximately 8 and 15 years. These two planets would have been closer to the binary in the past. This suggests that either these two planets have survived the CE ejection or that they have formed in the material ejected by the CE interaction (Mustill et al., 2013).

There is some diversity in all these phenomena: some are single companions orbiting around a post-giant primary too close yet too far, some are two companions around a post-giant, and some are a pair of planets around a close, post-CE binary. The common feature to all these systems is that the companion(s) avoided a dramatic in-spiral, yet are today located close enough to the primary that one must wonder how it (they) got to its (their) current location in the face of what must have been a large primary in the past or worse, a fully-fledged CE interaction ejecting copious mass.

1.4   The role of tertiaries in the CE interaction: this work

Approximately 20 − 30% of all binary systems are actually members of a triple system (Tokovinin et al., 2006; Rappaport et al., 2013). The fraction of triples is even larger in more massive stars (Sana et al., 2012). The presence of an outer companion in orbit around a binary system can significantly influence the evolution of that binary system. An outer companion can cause the period of an inner binary to shrink via Lidov-Kozai Cycles (Kozai, 1962; Fabrycky & Tremaine, 2007). Akashi & Soker (2017) suggested that 'messy' PNe (PNe that lack any form of symmetry) could arise from a triple system interaction. How a triple system functions in the context of a CE interaction has never been studied before.

Staff et al. (2016b) simulated the interaction between an RGB star and a planet and found that even massive planets are unable to disrupt the star and survive the interaction. They instead merge with the core. On the other hand they carried out a preliminary simulation (analysed in this work as part of the thesis) with two planets that appeared to lead to a somewhat stable orbit of the outer planet. Since we know that a single planet merges with the star, we wonder whether a second planet orbiting farther out, but still in range of the interaction, could survive because of the "sacrifice" of the inner planet.

On the other hand, the class of post-AGB stars discovered by Van Winckel (2003) and Van Winckel et al. (2009) (Section 1.3.1) do not have an inner binary that could be responsible for preventing a more dramatic in-spiral of the companion observed today. However, we wonder if it is possible that these post-AGB stars were triple systems at some point in the past and the inner companion merged with the primary. We wonder to what extent the inner merger may have played a role in allowing the outer companion to fall into today's orbit.

Similarly we wonder whether the triple configuration of PSR J0337+1715 played a significant role in the lack of in-spiralling of the outer companion (tertiary).

In Chapter 2 we describe the process of simulating the CE interaction using hydrodynamic codes. Then in Chapter 3 we describe the set-up and present the results of a simulation involving a RGB star and *two* planets. In Chapter 4 we describe a CE simulation of a 9.9 $M_\odot$ star with two stellar companions aimed at understanding the pulsar system. Finally in Chapter 5 we will present my conclusions and the options for future work.

2

Simulating the common envelope

As described in Chapter 1, the CE interaction is incredibly important to understand various astrophysical phenomena. The CE interaction is the basis upon which we understand the formation of compact, evolved binaries, such as SNe Ia progenitors. To create a model of the CE interaction we carry out 3D hydrodynamical simulations. The simulations are required to be 3D as the lack of symmetries prevents 1D models of the CE interaction. In terms of the physics, self-gravity and an ideal gas equation of state are included in these simulations.

In this chapter we will introduce the main techniques used to carry out hydrodynamic simulations, including a Lagrangian technique (Smooth Particle Hydrodynamics - SPH) and an Eulerian technique. We will also present previous simulations of the CE interaction.

2.1 Hydrodynamic simulations

The CE interaction occurs on a very short time scale, and is inherently asymmetric. Any hydrodynamic model therefore needs to be 3-dimensional (3D). The goal of these hydrodynamic simulations is to predict the parameters of post-CE systems given pre-CE binary parameters.

In general hydrodynamic codes solve a set of hydrodynamic equations. These equations describe the properties of a fluid and changes in the density, momentum and energy over time. More specifically they are:

$$\frac{\partial \rho}{\partial t} + \nabla \cdot (\rho \mathbf{v}) = 0 \tag{2.1}$$

$$\frac{\partial \mathbf{v}}{\partial t} + (\mathbf{v} \cdot \nabla) \mathbf{v} = -\frac{1}{\rho}\nabla P - \nabla \phi_{\text{Grav}} \tag{2.2}$$

$$\frac{\partial u}{\partial t} + \mathbf{v} \cdot \nabla u = -\frac{1}{\rho}\nabla \cdot (p\mathbf{v}) - \mathbf{v} \cdot \nabla \phi_{\text{Grav}} \tag{2.3}$$

$$\nabla^2 \phi_{\text{Grav}} = 4\pi G \rho \tag{2.4}$$

$$u_{\text{int}} = \frac{1}{\gamma - 1}\frac{P}{\rho} \tag{2.5}$$

where, ρ is the density of the fluid, $\mathbf{v}$ is the velocity of the fluid, P is the pressure, ϕ_{Grav} is gravitational potential energy, u is the specific total energy, u_{int} is the specific internal energy, and t is time.

Eqs. (2.1), (2.2) and (2.3) represent the continuity of mass, conservation of momentum and the conservation of energy, respectively. Since the CE is self-gravitating, the gravitational potential term was added and appears in Eqs. (2.2) and (2.3) as determined by the Poisson equation (2.4). To close the system, an equation of state is needed. In these simulation an ideal gas equation of state (Eq. (2.5)) for a monoatomic gas ($\gamma = 5/3$) is used.

2.1.1 Eulerian grid codes vs. smooth particle hydrodynamics codes

Hydrodynamic simulations can be divided into two main classes: Eulerian grid codes and Lagrangian codes.

The Eulerian approach uses volume coordinates, which is analogous to a grid. We used the Eulerian grid code ENZO (O'Shea et al., 2004; Bryan et al., 2014) for our simulations as adapted to the CE
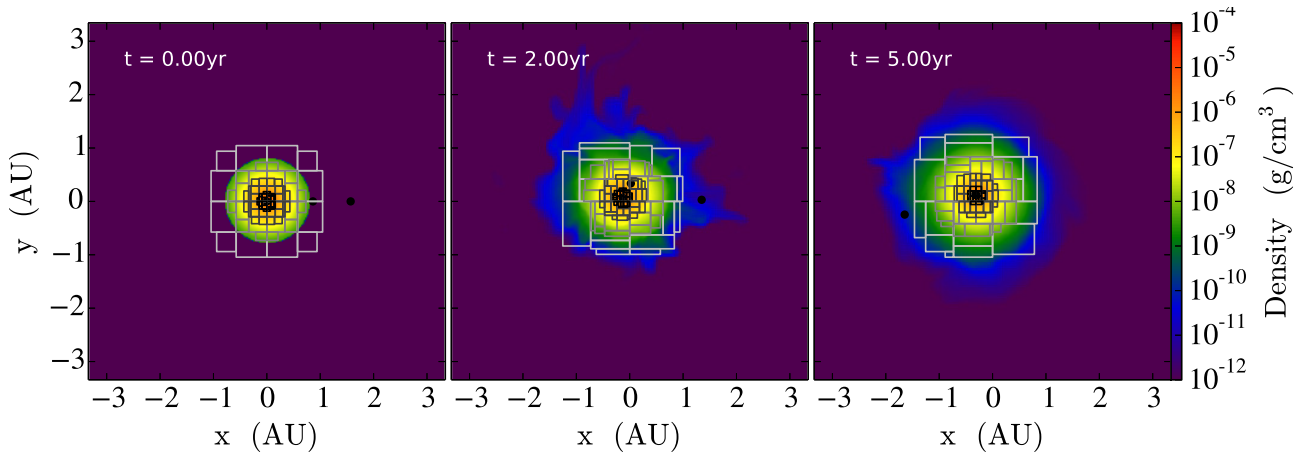
Figure 2.1: Density slices from an AMR ENZO simulation with 4 levels of refinement. The white, grey and black lines indicate the regions of higher refinement, with the black regions being the most refined. The refined grids change over the course of the simulation such that the most dense regions have the highest refinement. The figure was created using the visualisation package YT (Turk et al., 2011).

problem by Passy et al. (2012b) and Passy & Bryan (2014). In the Eulerian regime, quantities such as mass, momentum and energy are advected through the grid cells. The resolution of the simulation is limited by the size of the grid cells.

Adaptive Mesh Refinement (AMR) is a technique that has been developed for grid codes (including ENZO) to increase the resolution of the simulation where needed, rather than increasing the total number of cells over the entire domain. AMR involves creating refinement regions according to some criteria, such as the distribution and density of the gas. The higher the density the higher the level of refinement. See Fig. 2.1 for an example of the grid structure in an AMR-ENZO simulation.

The Lagrangian technique does not use a grid. The system is represented instead by particles of fluid. In SPH, mass coordinates are used to track these particles and their movement with respect to each other is followed. We used the SPH code PHANTOM developed by Price et al. (2017). Particles in SPH simulations have volumes that are inversely proportional to their density. SPH has the advantage of not requiring a grid, meaning that there is no mass or energy loss due to fluid leaving the grid like in Eulerian grid-codes. However, since in PHANTOM the particles have equal mass, SPH has a much lower resolution at lower densities, as the particles are smoothed over a larger area.

A summary of the strengths and weaknesses of the Eulerian and Lagrangian techniques is shown in Table 2.1. Due to the complementary strengths and weaknesses of the Eulerian and Lagrangian techniques we have used both types of codes in our simulation.

	Eulerian	Lagrangian
Strengths	– Has better resolution in low density regions that form in the CE. – Has a long history in computational physics. Schemes already developed to model shocks and radiative transport.	– Ideal for problems that trace mass such as ejecta from the CE interaction. – Physical quantities such as mass, energy, linear and angular momentum are better conserved.
Weaknesses	– Mass can leave the box which makes tracing CE ejecta difficult. – The re-zoning of AMR grids can lead to non-conservation of energy and density, and non-continuity of pressure-gradients.	– Low-mass regions that have been ejected from the CE can suffer from poor resolution. – Dynamical instabilities such as Kelvin-Helmholtz instabilities are occasionally poorly resolved.

Table 2.1: A summary of the strengths and weaknesses of the Eulerian and Lagrangian techniques in hydrodynamic simulations of the CE interaction.

2.1.2 The hydrodynamic codes ENZO and PHANTOM

Enzo is a parallel 3D hydrodynamic AMR Eulerian grid code that was originally used for cosmological simulations (O'Shea et al., 2004; Bryan et al., 2014; Passy & Bryan, 2014). Enzo is able to perform both hydrodynamic and N-body simulations. Passy et al. (2012b) modified Enzo to model the CE interaction by enabling Enzo to map a 1D radial profile from a stellar evolution code such as *Modules for Experiments in Stellar Astrophysics* (mesa, Paxton et al., 2011, 2013) to a 3D stellar model and introduced point masses with an analytical potential.

In Enzo we use point particles to represent very dense regions such as the primary's core and the companion stars or planets. These particles only interact with the gas and other particles gravitationally. For these point particles we use a smoothed gravitational potential, meaning that at large separations the gravitational potential is very close to the exact values given by the standard $\phi \sim r^{-1}$. However, at small separations of the order of the "smoothing length" the interactions become significantly weaker, and the potential is flat. This is done for numerical reasons: when two particles are very close to each other, or when a particle is very close to a cells centre, the gradient of the gravitational potential becomes arbitrary steep. Poorly sampled steep gradients cause energy conservation issues in hydrodynamical codes. By smoothing the gravitational potential it is possible to avoid some of these
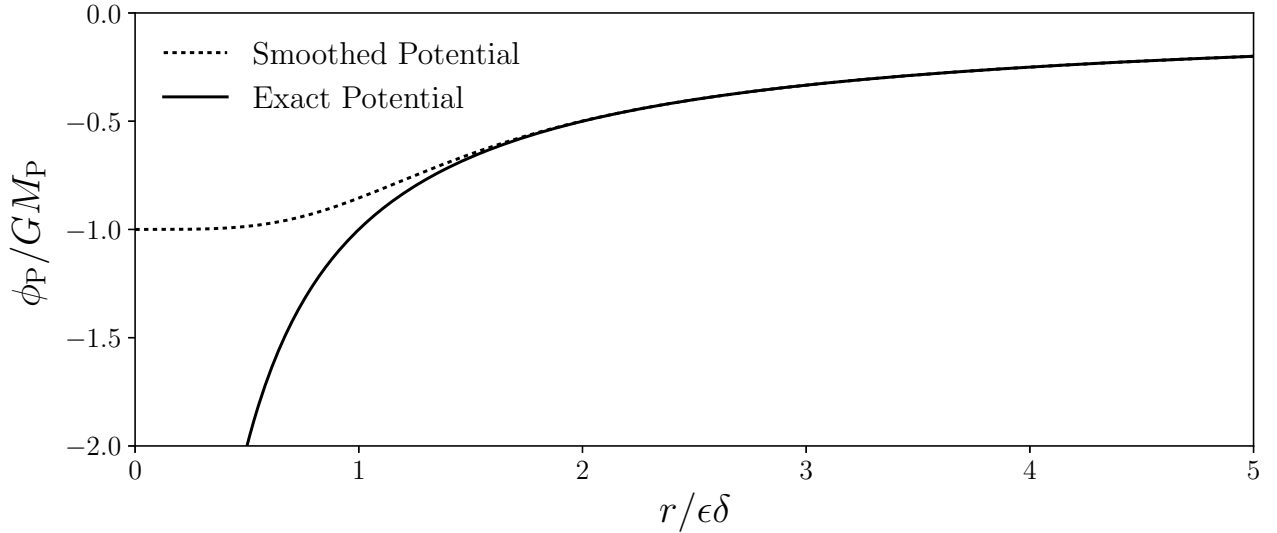
Figure 2.2: A comparison between the exact potential and the smoothed potential used in ENZO (Ruffert, 1993; Passy et al., 2012b). The solid line is the exact potential from a point particle given by $\phi \sim r^{-1}$. The dotted black line is the smoothed potential as shown in Eq. (2.6) with $\epsilon\delta = 1$.

conservation problems. The smoothed potential used in ENZO is given by Ruffert (1993):

$$\phi_{\mathrm{P}}(r) = -\frac{GM_P}{\sqrt{r^2 + \epsilon^2\delta^2 \exp\left[\frac{-r^2}{(\epsilon\delta)^2}\right]}} \, , \qquad (2.6)$$

where ϕ_{P} is the particle potential, M_{P} is the mass of the particle, G is the gravitational constant, r is the distance from the particle, δ is the size of the smallest cell, and ϵ is the number of cells over which the smoothing occurs (Fig. 2.2).

PHANTOM is a 3D hydrodynamic SPH code (Price et al., 2017) that was originally developed to model star formation, but has since been expanded to simulate a wide array of astrophysical problems. Iaconi et al. (2017b) modified PHANTOM to allow the code to create 3D stellar models from 1D radial profiles enabling it to perform CE interaction simulations. In a similar manner to ENZO, in PHANTOM we use point masses to simulate the core of the primary and the companions. A smoothed potential similar to the one shown in Eq. (2.6) is also implemented in PHANTOM.

2.2   Previous common envelope simulations

Not many CE simulations have been carried out in the last 20 years. (e.g., Rasio & Livio 1996; Sandquist et al. 1998; Ricker & Taam 2008, 2012; Passy et al. 2012b; Nandez et al. 2015; Kuruwita et al. 2016; Ohlmann et al. 2016a,b; Nandez & Ivanova 2016; Staff et al. 2016a,b; Iaconi et al. 2017a,b). In all these simulations the set-up involves placing a companion at or near the surface of a non-rotating giant star. The simulations are then evolved in their choice hydrodynamic code until the companion

has sufficiently in-spiralled. At the end of the simulation, the post-CE parameters such as the final separation and the total unbound mass are then determined. However, all simulations are limited in one way or another.

These simulations often use non-physical initial conditions. In particular, the companions are almost always positioned at a distance from the primary such that the primary is grossly outflowing its own Roche lobe (Passy et al., 2012b; Ricker & Taam, 2012). This configuration is used to significantly reduce the computational time required as the timescale of the mass transfer phase of the CE interaction is much longer than the in-spiral phase. Iaconi et al. (2017b) performed a simulation with a much more realistic initial separation and found that the post-CE separation was larger and slightly more mass was unbound.

Very limited coverage of the parameter space has been explored: Iaconi et al. (2017b) showed that the vast majority of common envelope simulations use a primary star with mass between $0.88 - 2M_\odot$ and there are no simulations with a primary mass grater than $5M_\odot$. All previous simulations have been restricted to binaries, and as a result there is zero attempts to determine the result of a CE interaction that involves three bodies.

In all CE interaction simulations that include only gravitational energy, very little of the CE is unbound (Iaconi et al., 2017b). As the orbital in-spiral occurs, the envelope is lifted from the binary and the separation stabilises however only of the order of 10% of the lifted envelope is unbound. As showed by Kuruwita et al. (2016) the lifted envelope could return as a "fall-back disk" which reduces the orbital separation further, but it fails to unbind the gas. These simulations suggest that an additional energy source is required to unbind the envelope, otherwise all CE interactions would result in a merger.

Nandez et al. (2015), Nandez & Ivanova (2016) and Ivanova & Nandez (2016) recently showed that by including the energy released by hydrogen and helium nuclei recombining with electrons in the expanding and cooling envelope (termed "recombination energy"), it is possible to unbind all of the envelope. However, what is unclear is whether all this energy is available to do work, or whether some escapes as radiation. Since neutral hydrogen is virtually transparent, some of this recombination energy could escape and thus that energy would not assist in unbinding the envelope.

Staff et al. (2016b) are the only ones to simulate the interaction between a giant star and planets. They found that even massive planets ($\sim 10M_J$) are unable to disrupt the star. As a result they do not survive the interaction, merging eventually with the core of the primary.

The role of magnetic fields is also not very well understood. Ohlmann et al. (2016b) performed the first magnetohydrodynamic simulations of the CE interaction. They report that the magnetic

fields appeared to play no role in the overall dynamics of the interaction, but found that fields were amplified to a strength of 10 -100 kG. The magnetic fields that Ohlmann et al. (2016b) reached in their simulation are similar to values determined from observational data of jets from post-CE binaries in PNe (Tocknell et al., 2014). The dynamical impact of magnetic fields is still an open question.

Although there have been a few attempts to understand the CE interaction using hydrodynamic simulation our ability to match observations is still extremely limited.

In Chapter 3 and Chapter 4 we will explore the CE interactions with 2 companions at two ends of the mass spectrum: a 0.8 $M_\odot$ RGB star with two 10 M_J planets and a 10 $M_\odot$ red super giant with two, solar-mass companions. In so doing we will explore some of the questions posed in Chapter 1.

3

Two-planet simulation

In Chapter 1 we posited that a third body acting in the context of a CE interaction may play a key role in the evolution of the system. Staff et al. (2016b) found that a CE interaction between a single massive planet and a 3 $M_\odot$ RGB or AGB star, results in a merger. Staff (in private communication) also carried out two additional simulations involving a giant star with a lower mass of 0.77 $M_\odot$ and one or two, 10 M_J planets, in order to test the effect of planets on a lower mass star. These simulations were never analysed. They form the basis of our investigation.

SIM1, SIM2 and SIM3 (Table 3.1) were performed by Jan Staff in 2016. SIM4 and SIM5 were performed by the Author. SIM6, carried out with PHANTOM, was performed by Thomas Reichardt under the direction of the Author and analysed fully by the Author. All plots and analysis was performed by the Author.

Table 3.1: Parameters for the simulations in this chapter. All simulations have $M_1 = 0.77\ M_\odot$

Sim. No.	Code[a]	n[b]	Resolution [c]	τ_{run}	M_{core}	M_2	a_2/R_* [d]	M_3	a_3/R_* [d]
			($R_\odot$ or part.)	(yrs)	($M_\odot$)	(M_J)		(M_J)	
SIM1	a-grid(E)	1	1.4	0 - 13.6	0.455	10	1.1	–	–
SIM2	a-grid(E)	2	1.4	0 - 14.3	0.455	10	1.1	10	2.0
SIM3	a-grid(E)	1	1.4	5.6^e - 23.1	0.455	–	–	10	1.75
SIM4	a-grid(E)	1	1.4	4.0^e - 11.0	0.455	–	–	10	1.86
SIM5	a-grid(E)	1	1.4	5.6^e - 8.9	0.465	–	–	10	1.75
SIM6	SPH(P)	2	80k	0 - 11.4	0.455	10	1.1	10	2.0

[a] a-grid: adaptive mesh refinement grid, SPH: smooth particle hydrodynamics, E: ENZO, P: PHANTOM.

[b] The number of planets in the simulation.

[c] Smaller is better for a-grid, larger is better for SPH.

[d] R_* is the radius of the primary. In all simulations $R_* = 169\ R_\odot$ except SIM6 where $R_* = 165\ R_\odot$. a_2 and a_3 are the orbital separation between the core and the innermost planet and the core and the outermost planet, respectively.

[e] Restarted time, measured from the beginning of SIM2.

3.1   Simulations background and set-up

These simulations expand on the work of Staff et al. (2016b) and introduce a second companion farther out from the primary. In Staff et al. (2016b), the planet is unable to survive the interaction with its 3 $M_\odot$ giant star and merges with the core. SIM1 (Table 3.1) uses a less massive primary (a 0.77 $R_\odot$, RGB star) to determine if a less massive giant could be "disturbed" more than a 3 $M_\odot$ one. SIM2 (Table 3.1) is the same as SIM1, but contains a second massive planet farther out, to see if the addition of a second planet could help change the outcome of the interaction.

SIM1 - SIM5 (and SIM7 see Chapter 4) were performed on the supercomputer RAIJIN at the National Computing Infrastructure in Canberra, Australia. These simulations utilised 128 cores. Since PHANTOM is not yet able to perform CE simulations in parallel clusters, SIM6 was performed on a server at Macquarie University with 88 cores.

3.1.1   Initial conditions

SIM1 - SIM5 were performed using ENZO in a cubic box with a side length of 6.68 AU (1437 $R_\odot$). Each simulation utilises AMR with 4 levels of refinement, with each level having a refinement factor

of 2 (i.e., each cell is divided into 2 along each of its dimensions for each level of refinement). The coarse grid has a resolution of 128 cells per side (cell size of $11.2\,R_\odot$). The refinement occurs in the coarse grid when the density in the cell is greater than 9.5×10^{-10} g/cm^3. The smallest cell has a size $\delta = 1.40\,R_\odot$. Staff et al. (2016a) found that using smoothing length of $\epsilon = 3$ resulted in better energy conservation in their simulations. Due to the similarity between Staff et al. (2016a) and these simulations, a smoothing length $\epsilon = 3$ was also used in all of the ENZO simulations. The length scale of the smoothed potential is $4.2\,R_\odot$.

The stellar model was created using the one-dimensional stellar evolution code MESA (Paxton et al., 2011, 2013). A $1\,M_\odot$, zero-age main sequence, solar-metallicity ($Z = 0.02$) star was evolved in MESA until the model was 12.34 billion years old. The model is an RGB star with a radius of $169\,R_\odot$ with a mass of $0.77\,M_\odot$.

The 1D stellar model is then mapped into the 3D computational domain. Since the resolution of ENZO is much lower than that of MESA models, the core of the star, where most of the mass is concentrated, is not resolved, resulting in a mass deficit. To account for this, a point particle is added to the centre of the star with a mass equal to the missing stellar mass. In these simulations the core has a mass of $0.455\,M_\odot$ (the actual core in MESA has an almost identical mass of $0.458\,M_\odot$) and the gas has a mass of $0.319\,M_\odot$.

Unlike MESA, ENZO does not account for the stellar micro-physics. It instead uses an ideal gas equation of state. With the addition of a massive point particle as a core and a smoothed gravitational potential, the star is not in perfect hydrostatic equilibrium. Following the method described in Passy et al. (2012b) and Iaconi et al. (2017b), the velocities of the gas are damped for a few dynamical times (of the order of a few years) to force the star to relax into its hydrodynamic equilibrium. The structure is then evolved for a further few dynamical times without damping, to check for stability.

In SIM1 and SIM2 the point masses used to represent planets have a mass of $10\,M_J$. The initial configuration of SIM1 has a planet placed near the surface of the star at $186\,R_\odot$ (1.1 times the radius of the primary) from the core. The planet and star are placed in Keplerian orbits with an initial velocity in the y direction of -0.346 km/s for the RGB star and $+28.3$ km/s for the planet.

SIM2 is similar to SIM1 except it also has a second planet placed at $338\,R_\odot$ (2.0 times the radius of the primary). Using an N-body integration code that we wrote, described in Section 4.1.4, we ensured that the 3 body orbits were not inherently unstable over the time of the simulation. These planets are placed on the same side of the core in co-planar orbits. Whilst the outer planet in SIM2 was placed on a Keplerian orbit with an initial velocity in the y direction of $+20.8$ km/s, the inner planet was
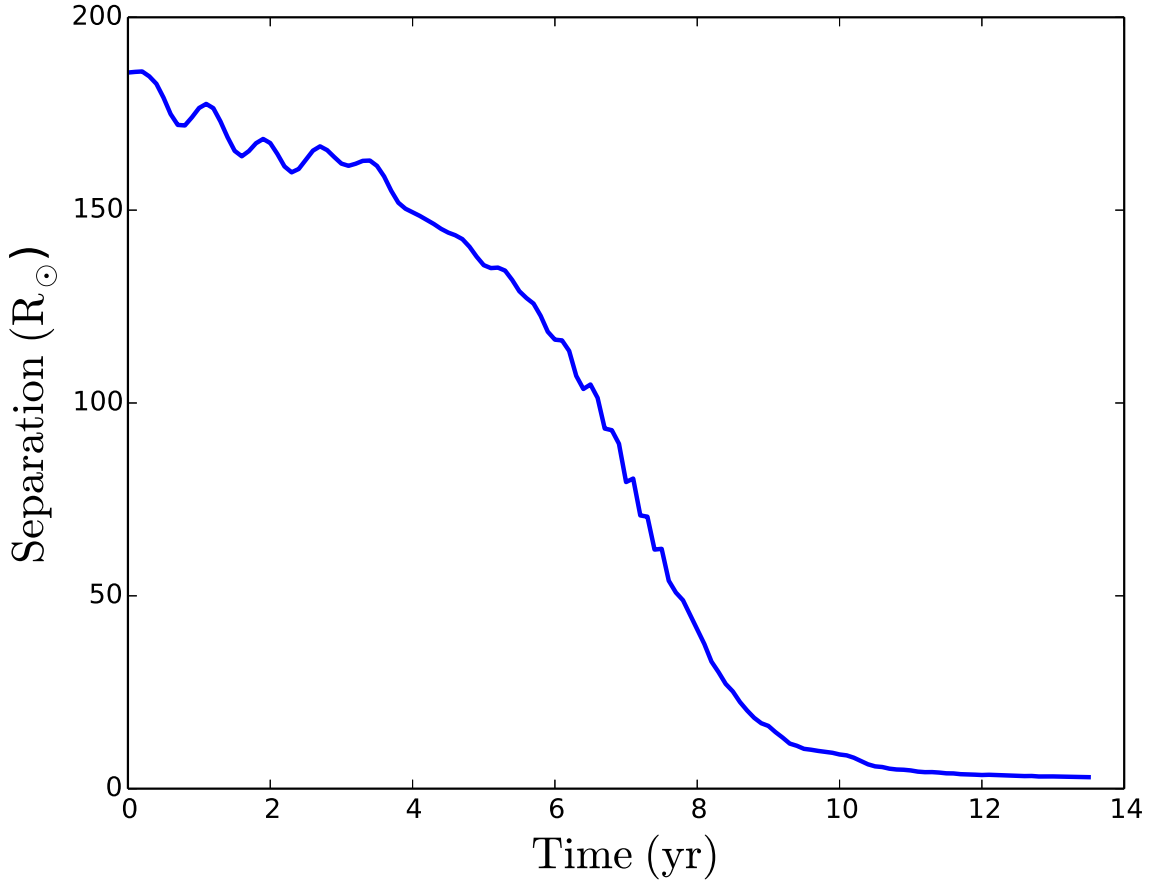
Figure 3.1: The separation between the stellar core (0.455 M$_\odot$) and the planet (10 M$_J$) in SIM1.

erroneously placed in orbit with the same velocity as the outer planet. Since the inner planet has a velocity that is $\sim 26\%$ slower than Keplerian, the inner planet begins on an elliptical orbit. This orbit causes the inner planet to in-spiral more rapidly than it otherwise would if the orbit were circular. As we will explain below, we do not believe that a more rapid in-spiral had an effect on our conclusions.

SIM6 is an SPH simulation identical to of SIM2 using PHANTOM with a resolution of 80,000 particles, but where both planets were correctly placed on Keplerian orbits (+28.3 km/s and +20.8 km/s for the inner and outer planets, respectively). This simulation confirms that our conclusions are not affected by the sub-Keplerian orbit of the innermost planet in ENZO and provides us with additional verification checks. The SPH control simulation was started early on in the project, however due to PHANTOM's speed, the 6 month computational time meant that the results only became available towards the end of the project.

3.2   Results: an RGB star with one or two massive planets

SIM1 contains a single planet initially situated near the surface of the primary star. Fig. 3.1 shows the separation of the planet as it in-spirals towards the the stellar core. The orbital evolution is similar to what is observed by Staff et al. (2016b) with a more massive giant. The final separation in SIM1 is 9 $R_{\odot}$, which is of the same order as the smoothing length. This and the fact that the stellar structure is minimally affected by the in-spiral indicates that a merger between planet and giant core is likely. Almost no gas is unbound, such that one would conclude that a lower mass giant does not change the conclusions reached by Staff et al. (2016b) for a more massive giant.

In SIM2 the radius of the star's Roche lobe with respect to the innermost planet is 132 $R_{\odot}$, which is much less than the stellar radius (169 $R_{\odot}$). Thus the star is massively overflowing its Roche lobe, which leads to instantaneous RLOF onto the inner planet. As shown in the density slices in Fig. 3.2 and Fig. 3.4, the inner planet is engulfed by the envelope of the primary and the in-spiral phase begins immediately.

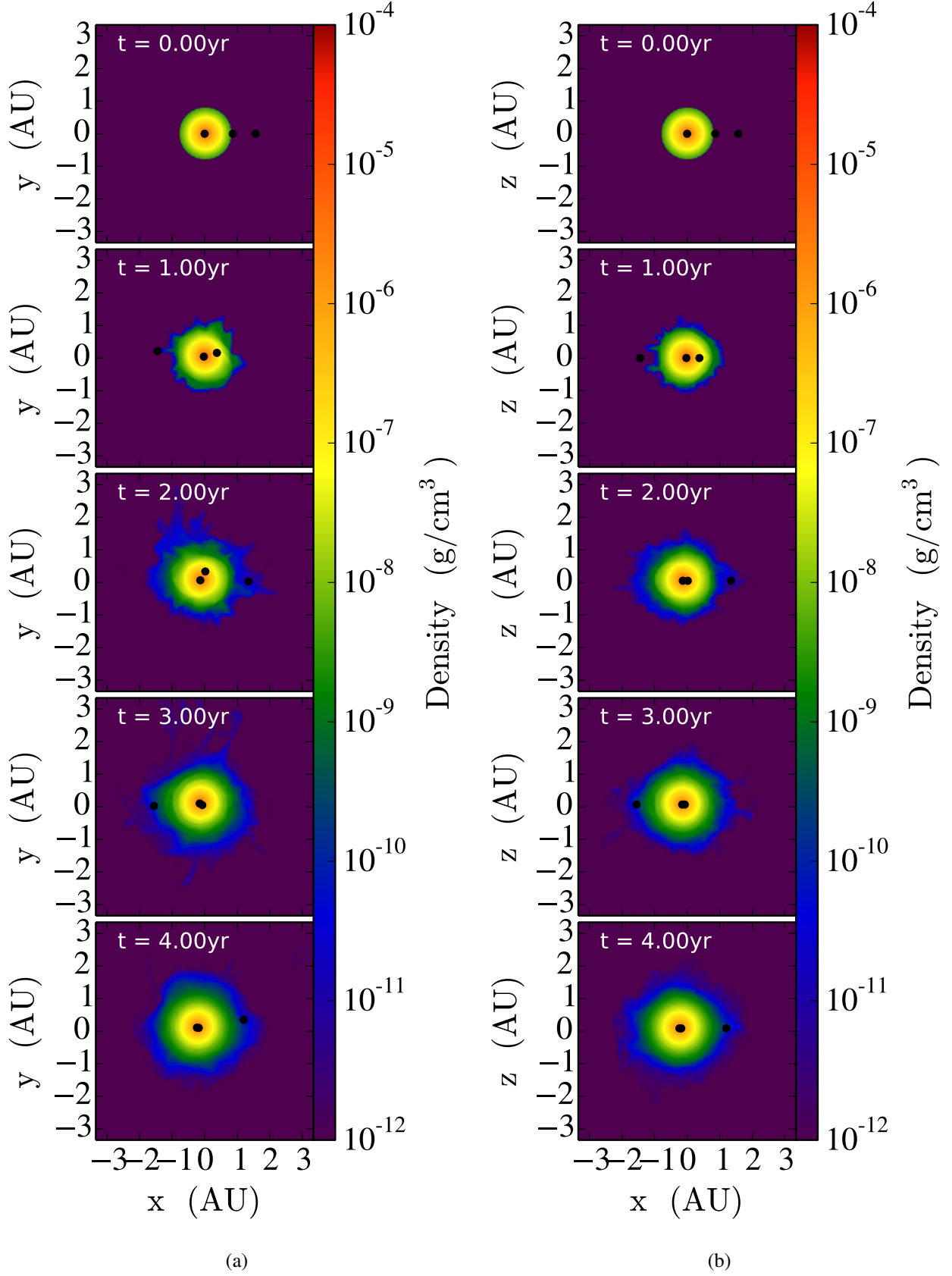(a)   (b)

Figure 3.2: (a) Density slices along the orbital plane after from top to bottom 0, 1, 2, 3 and 4 years from the beginning of SIM2. The core of the primary and the two planetary companions are represented as the black dots. The size of the points is not indicative of any physical property of the planets. (b) Density slices perpendicular to the orbital plane (x-z) at the same times as in (a).

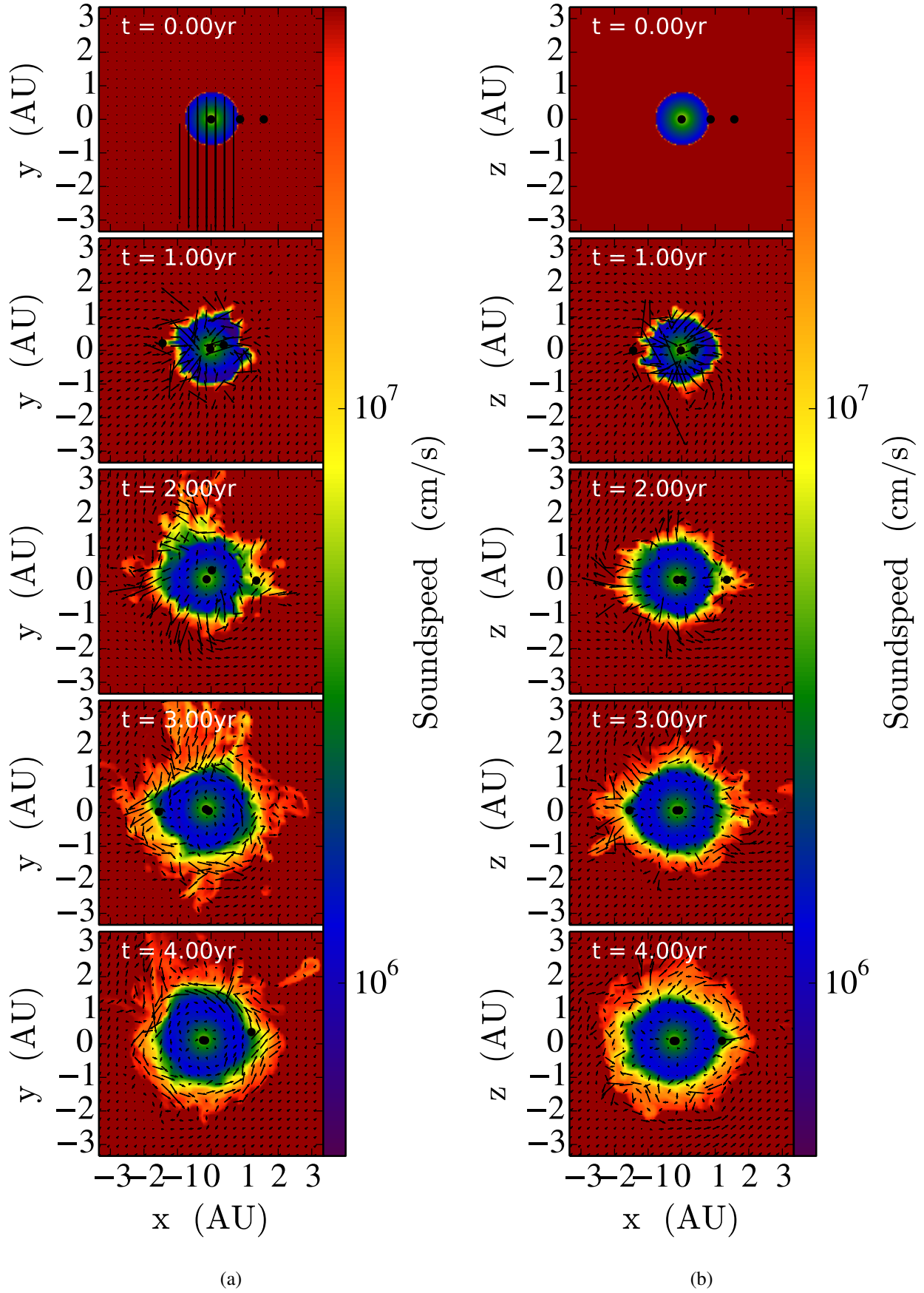(a)   (b)

Figure 3.3: (a) Sound speed slices along the orbital plane after from top to bottom 0, 1, 2, 3 and 4 years from the beginning of SIM2. The black vectors represent the velocity field of the envelope. (b) Sound speed slices perpendicular to the orbital plane (x-z) at the same times as in (a).
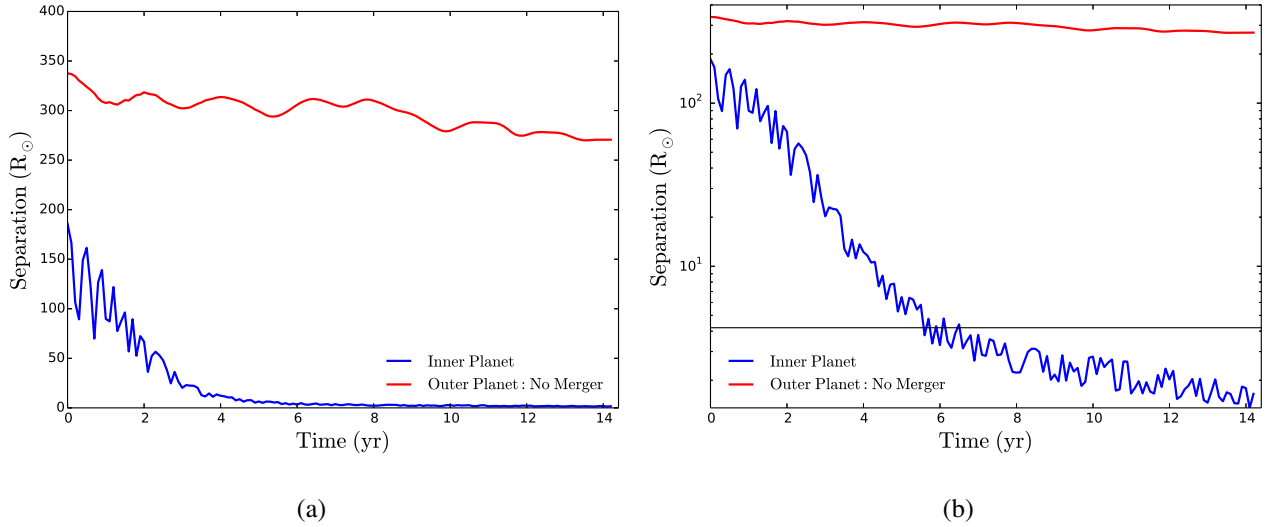
(a)   (b)

Figure 3.4: (a) the separation between the stellar core (0.455 $M_\odot$) and the two planetary companions (10 M_J) throughout the 14.3 year simulation. (b) The same as the left-hand side but with a log-scale y-axis. The inner and outer planets initially have separations of approximately 186 $R_\odot$ and 338 $R_\odot$, respectively. The black line horizontal indicates the smoothing length of the simulation (4.2 $R_\odot$).

3.2.1   Orbital evolution

The orbital separations between the core of the primary and the two planets are shown in Fig. 3.4. The inner planet is placed in orbit at the stellar radius (186 $R_\odot$, as is typically done in CE simulations, e.g., Iaconi et al., 2017b). The planet is rapidly engulfed by the primary star. After 4 years the orbital separation has shrunk to 12 $R_\odot$, a reduction of approximately 94%. At that time the inner planet's in-spiral slows dramatically as it approaches the smoothing length. Once it reaches the smoothing length the inner planet experiences a much weaker gravitational force and thus the in-spiral is slowed.

The outer planet does not experience a sudden in-spiral. Instead it maintains an orbital separation of approximately 300 $R_\odot$, with a very gradual decay over 14 years (Fig. 3.4). The outer companion is embedded in a low, but not insignificant density. Over the relatively long 14 years of the simulation, we would expect to see a more significant in-spiral. However this lack of a significant in-spiral could be the result of weaker drag forces and/or radially moving gas (see Section 3.2.3).

3.2.2   Energy and angular momentum conservation

The simulations of Staff et al. (2016b) displayed reasonable energy and angular momentum conservation properties. Enzo does not conserve energy and angular momentum implicitly and strong gradients in any of the physical quantities such as internal energy or density can result in energy non-conservation. Gradients are usually large near the core point mass. In Fig. 3.5 we show the
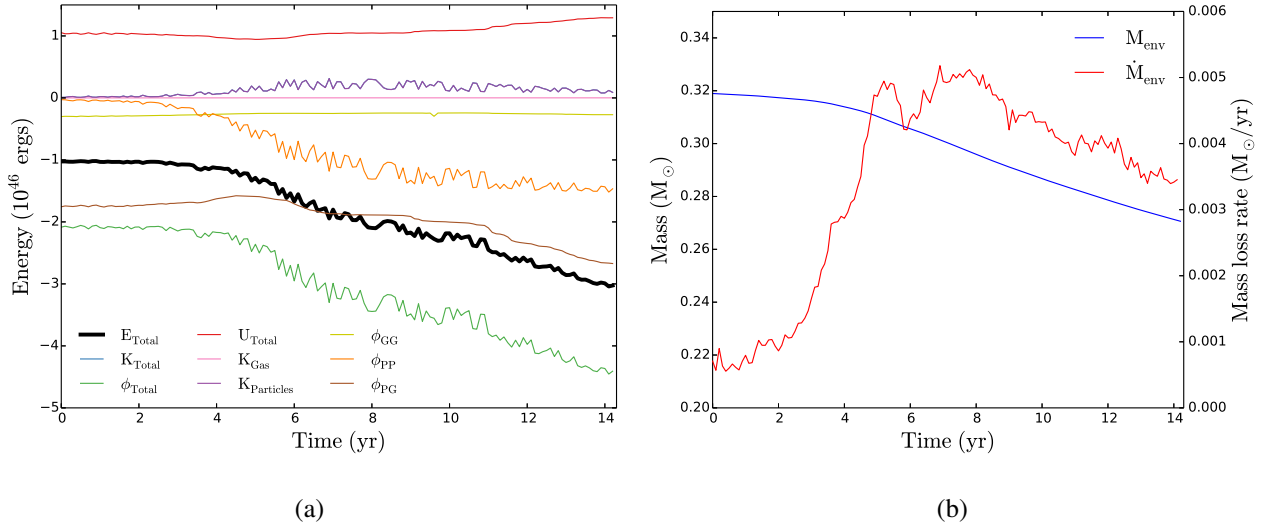
Figure 3.5: (a) The total energy and energy components as function of time for SIM2. E_{Total} is the total energy, K_{Total} is the total kinetic energy, K_{Gas} is the kinetic energy of the gas, $K_{Particles}$ is the kinetic energy of the companions and primary core, ϕ_{Total} is the total potential energy, ϕ_{GG} is the potential energy gas-to-gas, ϕ_{PP} is the potential energy particle-to-particle, ϕ_{PG} is the potential energy particle-to-gas, U_{Total} is the total thermal energy. Since the kinetic energy of the gas is almost zero, the total kinetic energy is dominated by the kinetic energy of the particles. (b) Total envelope mass (M_{env}) and envelope mass loss rate ($\dot{M}_{env}$) of the envelope for SIM2.

various energy components including kinetic energy, potential energy and thermal energy. The kinetic energy of the particles and of the gas is calculated using:

$$K_\alpha = \frac{1}{2} \sum_i m_i v_i^2 \tag{3.1}$$

where K_α is the kinetic energy component (particle or gas), m_i and v_i are the mass and the velocity magnitude of the particle or gas cell respectively. The total kinetic energy is calculated by summing the two kinetic energy terms for the particles and the gas. The potential energy is calculated using:

$$\phi_\alpha = -\frac{G}{2} \sum_i \sum_j \frac{m_i m_j}{r_{ij}} \tag{3.2}$$

where ϕ_α is the potential component, G is the gravitational constant, m_i and m_j are the masses of the particle or gas cell and, r_{ij} is the separation between m_i and m_j. The total potential energy is calculated by summing the three potential energy components: particle-to-particle (PP), particle-to-gas (PG) and gas-to-gas (GG).

SIM2 initially has total energy of -1.02×10^{46} ergs. As shown in Fig. 3.5a, the total energy is reasonably conserved in the simulation for approximately 5 years. After 5 years energy non-conservation starts to occur and the total energy becomes more negative, i.e, the system becomes more bound. The decrease in the total energy must be due to an excessive decrease in the particle-gas potential energy. The kinetic energy of the gas remains at virtually zero for the entire simulation.

Figure 3.5b shows the mass of the envelope and the mass loss rate from SIM2. The decrease in total energy must be caused by a non-conservation in the particle-to-gas potential energy (since the decreasing particle-to-particle potential energy is calculated analytically). All previous ENZO simulations by our group displayed almost perfect mass conservation (except for the mass flowing out of the simulation domain boundary). However, upon checking mass conservation for this simulation we noticed that the outflow boundary conditions could only account for 80% of the mass loss from the domain over 14 years, namely 0.04 $M_\odot$, or 12% of the total envelope mass. The remaining 20% must be due to mass non-conservation, which can gauge at the 2.5% level. An analysis showed that there is mass-loss at the boundaries of newly formed sub grids. A loss of mass near the core, where the grids are spawned, would result in an increase of the (negative) potential energy, not a reduction. We are unable at this time to determine the origin of the non-conservation, but we suspect that the penetration of the inner planet below the smoothing length, which happens at approximately 6 years and corresponds to the approximate time of energy non-conservation, may have something to do with the problem. Alternatively it could be a bug in the script that measures the respective energy components of the particle-gas interaction from the simulation data[1].

To check that the main features of SIM2 are not due to this lack of conservation, an SPH simulation (SIM6) using PHANTOM was performed using the same set-up as in SIM2 with a resolution of 80,000 particles (and with the two planets correctly positioned in their respective Keplerian orbits). The resolution of SIM6 is average for typical SPH simulations of the CE interaction. However, the resolution tests carried out by Iaconi et al. (2017b) using 80,000 to 1 million particles show reasonable convergence.

Past SPH simulations with PHANTOM (Iaconi et al., 2017b) have exhibited better conservation properties than the equivalent ENZO simulations, so if energy or angular momentum non-conservation is causing any of the observed effects, and in particular the orbital stability of outer planet, then we should see a difference in the outcomes of the SPH simulation. As shown in Figs. 3.6a and 3.6b, energy and angular momentum are almost perfectly conserved in SIM6.

In SIM6 the inner planet takes much longer to begin its plunge towards the stellar core than in SIM2 (compare Fig. 3.4a for ENZO and Fig. 3.6c for PHANTOM). This is due to the elliptical nature of the inner planet's orbit in SIM2. Fig. 3.7 shows density slices of the z plane from SIM2 (ENZO) and SIM6 (PHANTOM) at 1.50 years and 7.17 years, respectively. These slices are taken when the inner planet is at similar orbital separations in their in-spiral (the SPH in-spiral is slightly more advanced). Since the

---

[1]All scripts for the analysis of this thesis had to be adapted to analyse three, instead of the typical two, particles. The way enzo keeps tracks of particles made it non-trivial to carry out the sums.
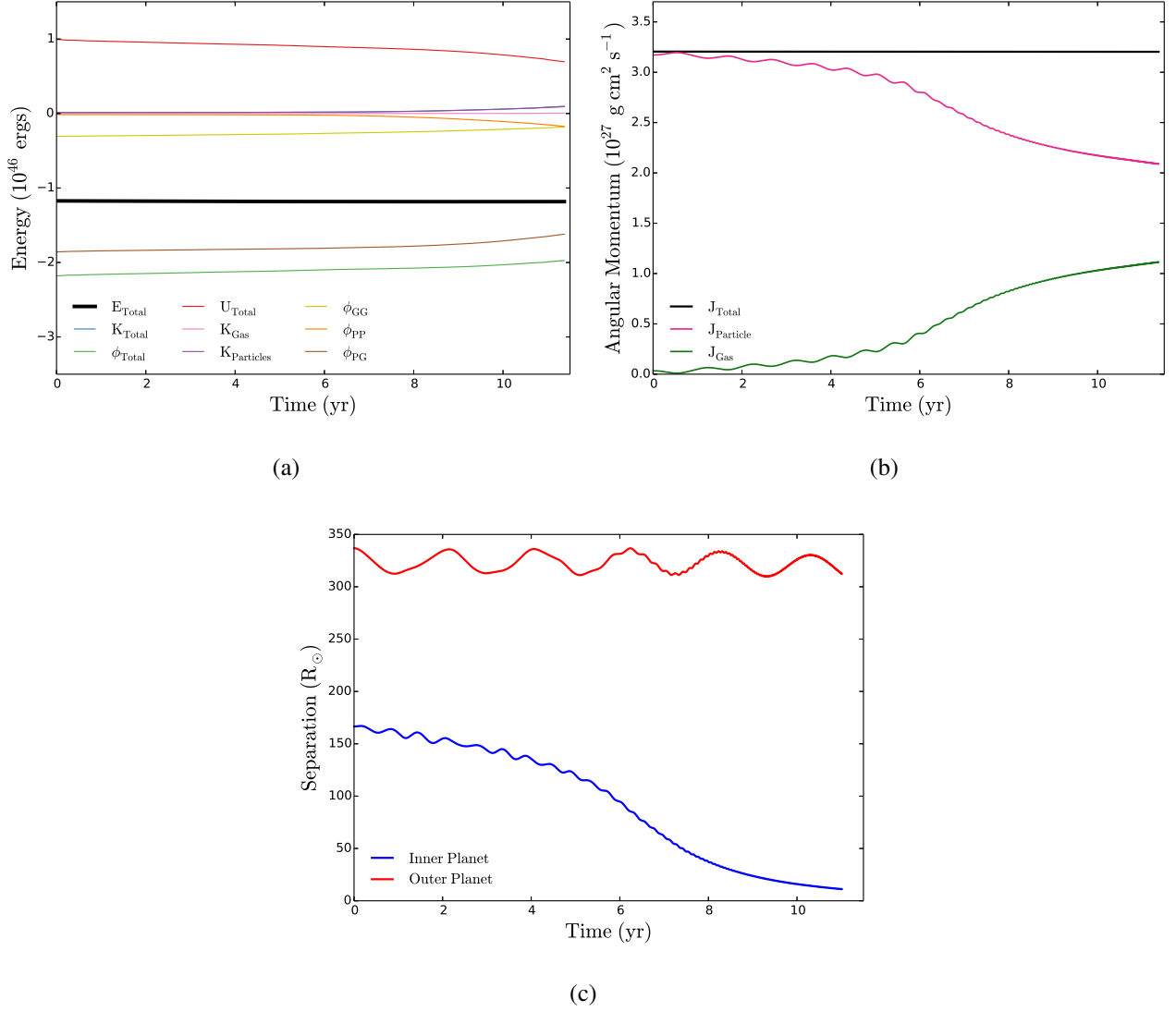
(a)

(b)

(c)

Figure 3.6: (a) The total energy and energy components for SIM6. The label are the same as from Fig. 3.5. (b) The total angular momentum from SIM6. J_{Total}, $J_{Particle}$ and J_{Gas} are the total angular momentum, the angular momentum of the particles and the angular momentum of the gas respectively. (c) The separations between the core of the primary and the two planets from SIM6.

outer planet has negligible impact on the inner planet's in-spiral, a fairer comparison of the properties of the inner planet's orbital evolution would be between SIM1 and SIM6: the in-spiral time scale for SIM1 and SIM6 (inner planet) are very similar, with a reduction in initial orbital separation of 85% by 8.4 years for SIM1 and 8.8 years for SIM6.

To compare SIM2 and SIM6 we need to remember that the orbital in-spiral is much faster in SIM2 because of the elliptical nature of the innermost planet's orbit. What we observe in the SPH simulation (SIM6) is that the outer planet orbit is stable, as is the case in the ENZO simulation. Arguably the SPH simulation does not extend for as long a time as the ENZO simulation. It is only carried out to the early end of the innermost planet in-spiral, rather than for several years after the end of the in-spiral as is
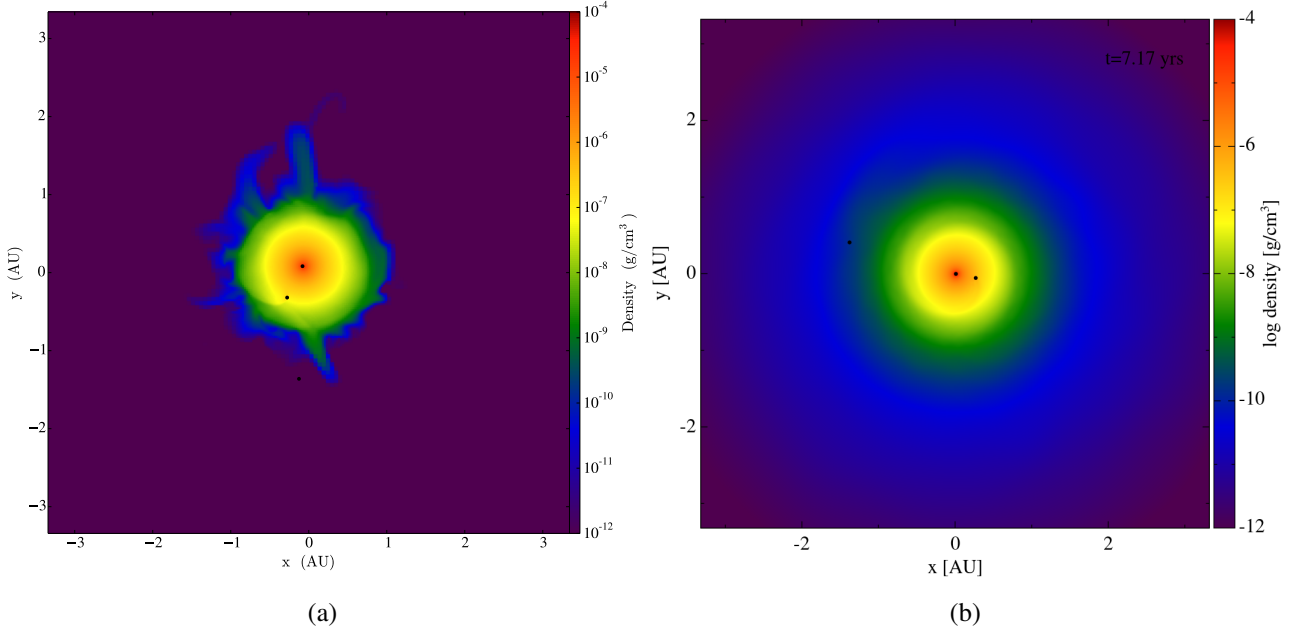
Figure 3.7: (a) Density slice from SIM2 at 1.5 years. (b) Density slice from SIM6 at 7.17 years. In both slices the the separation between the inner planet and the core is approximately 60 R$_\odot$.

the case in the ENZO simulation. The simulation is still running as this thesis is being written, so we will be able to confirm whether the orbit of the outer planet in the SPH simulation is quite as stable as in ENZO.

We also notice that the SPH star has a larger low density halo than the ENZO star by this time in teh simulation. This is partly due to the fact that the SPH star stabilises differently into the computational domain. As is also true in other simulations (Iaconi et al., 2017b) the SPH star is mapped from 1D and stabilised, but a few particles are outside of the stellar radius. In the case of Fig. 3.6 (b) we see that a density $\sim 10^{-11}$ g/cm^{-3} permeates a large volume. Since each SPH particle has a mass of 0.315 M$_\odot/80\,000 = 4 \times 10^{-6}$ M$_\odot$, we calculate that the low density halo contains approximately 100 particles. Finally, even assuming that the low density medium present in the SPH simulation but not in the ENZO simulation has an effect on the outer planet, it would have a destabilising effect and yet the orbit is stable.

Based on the analysis of our simulation data, and including caveats, there could be a number of reasons for the outer planet not in-spiralling more promptly. In Fig. 3.6 we can see that the outer planet does not in-spiral, but energy and angular momentum is almost perfectly conserved. This leads us to believe, though cautiously, that energy and angular momentum non-conservation do not play a role in the orbital stability of the outer planet. To put this conclusion on firmer ground we need (1) to establish the cause of the energy non-conservation in ENZO and (2) to run the SPH simulation for

approximately another 5 years of physical time, to test the orbital stability of the outer planet over the same time scale as the ENZO simulation.

Another cause of erroneous results can be resolution effects. We did not perform a convergence test. However, Staff et al. (2016b) did a convergence test for their simulations and Iaconi et al. (2017b) carried out convergence testing for the SPH simulations similar to SIM6. Staff et al. (2016b) found that an under-resolved simulation leads to an over estimation of drag forces. The Bondi radius (Bondi, 1951) of the outer planet at the start of the simulation is $\sim 8 \, R_\odot$, smaller but comparable to the coarse resolution of $\sim 11 \, R_\odot$. This resolution rapidly increases due to the additional grids that form near both planets. Even if the gravitational drag force were stronger in the simulation than in nature, this would contribute to more in-spiral of the outer planet, not stability. We conclude that the orbital stability is not due to lack of resolution, though a formal convergence test should be carried out (we note that convergence testing is highly problematic in this kind of extremely time-consuming simulations).

Could there be resonances between the inner and outer planet that could justify the orbital stability of the outer planet? There is nothing in the ENZO simulation that leads us to that conclusion. The high frequency motion of the inner planet's orbit is not reflected in the outer planet's orbit. However the dump frequency of the data of the ENZO simulation could hinder a proper analysis. On the other hand, we observe in Fig. 3.6c that after 5.9 years there appears to be a high frequency oscillation in the outer planet's separation, which has the same frequency as the oscillation of the inner planet's orbit. This oscillation also increases in frequency at the same rate as the orbital oscillations increase during the inner planet's in-spiral. This correlation between the high frequency oscillation in the outer and inner planet's separations, could mean that there is a kind of resonance in SIM6 between the inner and outer planet during the in-spiral. This may be evidence that the outer planet is directly affected by the inner planet during the CE interaction. We have recently involved an expert in dynamics into this discussion, Dr. Rosmary Mardling of Monash University, to help with the analysis of any interaction of this type.

3.2.3 Gas flow and drag forces

As shown in Eq. (1.2), the gravitational drag is dependent on density and the relative velocity between the gas and the planet. The drag is in the direction of the relative velocity vector, which in a typical in-spiral is in the direction opposite to the particle's orbital motion. An in-spiralling body usually experiences a drag that slows the orbital speed and promotes orbital reduction (see Chapter 1).

It may be possible, however, that outwards moving envelope gas, flung out because of the interaction
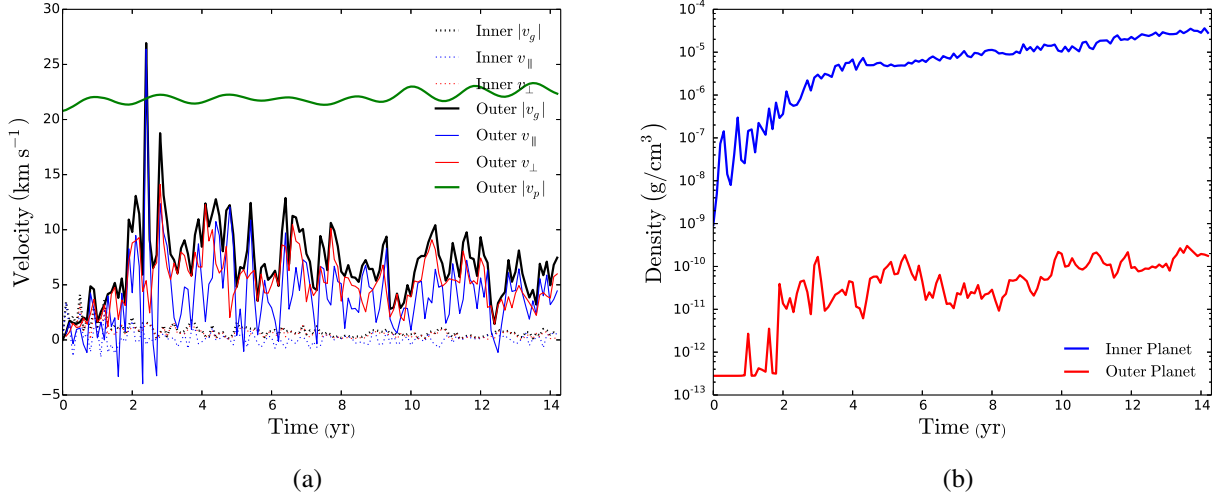
(a)   (b)

Figure 3.8: (a) The velocity components of the gas around the planets in SIM2. "Outer" and "Inner" refer to the outer and inner planets respectively. $|v_g|$ is the average velocity magnitude of the gas at the position of the planet, $v_{||}$ is radial component of $|v_g|$, $v_\perp$ is the component of $|v_g|$ perpendicular $v_{||}$, $|v_p|$ is the velocity magnitude of the planet. $v_{||}$ represents the outwards moving gas and $v_\perp$ represents the gas moving in the same direction as the planet. (b) The average density of the gas in the cells surrounding the planet as a function of time.

with the *inner* planet, is creating a radially outwards gravitational drag on the outer planet. This radial gravitational drag could be delaying the outer planet's in-spiral.

By decomposing the velocity of the gas in the orbital plane (the velocity perpendicular to the orbital plane is neglected) into radial and perpendicular components we can compare the gravitational drag on the planets in both these directions.

We selected a $3 \times 3 \times 3$ cell box centred on the location of each point mass planet. We then calculated the average of the 27 gas velocity vectors. This allowed us to compute the average velocity of the gas (with respect to the grid) parallel to the radial direction and perpendicular to that direction.

The velocity components $v_{||}$ and $v_\perp$ (the radial and perpendicular direction components, respectively) for both planets are shown in Fig. 3.8a. The overall velocity of the gas surrounding the inner planet (dotted lines) is small for the entire duration of SIM2 as expected: the planet in-spirals into the gas that is effectively at rest. This is what we should expect as the velocities of the gas are damped at the beginning of SIM2 and the relatively light planet has only a small impact on the stellar envelope. The orbital velocity of the inner particle with respect to the grid is not shown in this plot. However, its velocity ranges from around 40 km/s in the first 2 years before increasing to its peak velocity ($\sim$ 170 km/s) at 7 years.

Unlike the inner planet, the gas surrounding the *outer* planet has a fairly high velocity (> 5km/s). The

radial velocity component of the gas is typically positive indicating outwards gas flow at an average speed of ~ 5 km/s. The velocity component along the orbital direction is slightly higher, at ~ 7 km/s. The orbital velocity of the outer planet, on the other hand, is ~ 22 km/s. This means that the relative velocity of the gas with respect to the planet is 15 km/s in the direction against the orbital motion.

Overall there is a substantial outward component of the motion that is about one third of the component that creates the in-spiralling drag. However, it is an important caveat that the analytical formulation of gravitational drag is known to not capture the effects of density gradients (see Section 1.2).

The gravitational drag is also dependant on the density of the gas around the planet. In Fig. 3.8b we show the average density of gas that surrounds the two planets. Clearly the outer planet is embedded in gas with a density that is approximately 4 orders of magnitudes smaller than the inner planet. This significant difference in density partly justifies the lower drag on the outer planet. An rough order of magnitude estimation of the drag forces can be determined using Eq. (1.2). In a uniform density medium the ratio of the drag between the outer and inner planets is would be the ratio of the relative velocities. $F_{\text{outer}}/F_{\text{inner}} \sim \frac{v^2_{\parallel,\text{outer}}}{v^2_{\perp,\text{inner}}}$. After approximately 2 years the $F_{\text{outer}}/F_{\text{inner}} \sim \frac{5^2}{15^2} \sim 0.11$. However since the outer planet is in a lower density medium, the ratio of the drag forces is 1.1×10^{-5}.

It appears, in conclusion that there is a substantial component of the drag force in the outward direction and this may, at least in part, counter the inward drag caused by the in-spiralling motion. The test of whether this is what is balancing out the inward drag, is to determine the actual force against the orbital direction and the resulting change in angular momentum of the planet. Then we would compare this to the balancing force in the outward direction. This would have to be done following the technique of Staff et al. (2016b), which overcomes a series of problems that arise when measuring the needed quantities from simulation data.

3.3 The effect of the inner planet and core "merger"

As the inner planet gets close to the core, it approaches the smoothing length (4.2 $R_\odot$) of the gravitational potential. At this point the orbital evolution of the inner planet cannot be considered viable. It is likely that, in nature, the inner planet would merge with the core of the primary (see also Staff et al. (2016b)). To simulate this type of merger event we carried out two simulations (SIM3 and SIM4) by removing the inner planet at 5.6 years in SIM3 and 4.0 years in SIM4. Since the mass of the planet is small relative to the mass of the primary core, the mass was not added to the core.

The Roche limit is the minimum distance from a massive body that an object held together by its own gravity can exist without being torn apart by tidal forces. Hence the Roche limit of the primary's core

is the point at which the in-spiralling planet would break up. The Roche limit of an object is given by
Shu (1982):

$$
\begin{aligned}
d_{Roche} &= 1.26 R_s \left(\frac{\rho_s}{\rho_p} \right)^{\frac{1}{3}} \\
&= 1.26 R_p \left(\frac{M_s}{M_p} \right)^{\frac{1}{3}},
\end{aligned}
\tag{3.3}
$$

where d_{Roche} is the Roche limit of the star, R_s and R_p are the radii of the star and the planet, respectively,
M_s and M_p are the masses of the star and the planet, respectively. Finally, ρ_s and ρ_p are the densities
of the star and the planet.

Although our planets are point masses, in reality they have typical sizes. As shown in Bodenheimer
et al. (2001), all gas-giant exoplanets have a radius somewhat similar to the radius of Jupiter. The
exact radius is actually a function of the planet's distance from its host star, as the closer the planet is
the more it is heated and "puffed up". Typical gas giant exoplanets have radii in the range of $1 - 1.5$
that of Jupiter ($0.1 - 0.15 R_\odot$). Using these values of R_p we find that the core of our planet has a
Roche limit of $d_{Roche} \sim 0.46 - 0.69 R_\odot$. The planet will also break-up when it fills its Roche lobe. We
calculate that the planet will fill its Roche lobe at a separation between 0.77 $R_\odot$ and 1.2 $R_\odot$. From
these values we reason that the break-up radius of the planet is roughly on the order of 1 $R_\odot$.

This break-up distance is significantly smaller than the smoothing length of the gravitational potential
(4.2 $R_\odot$), hence we cannot follow the inner planet to its merger moment. However here as in Staff et al.
(2016b) we make the assumption that the in-spiral would continue because there is nothing to stop it:
neither the local density, nor the relative velocity of the planet and the local gas are decreasing, which
means that the gravitational drag on the planet should not diminish.

For this reason we decided to simulate a merger event by removing the inner planet as it was approaching
the smoothing length. In SIM3 the simulated merger occurred at $t = 5.6$ years. At this time the inner
planet has a separation of 3.8 $R_\odot$. We also tested a second merger (SIM4) at $t = 4.0$ years where the
companion has a separation of 12.2 $R_\odot$. This second time was chosen for three reasons: first, energy
is well conserved for the first 4 years; second, at 4 years the outer planet is situated in a lower density
medium than at 5.6 years and this may play a role. Third, because 4 years corresponds to the outer
planet being at orbital apastron (314 $R_\odot$) as opposed to the time of 5.6 years when it is at periastron
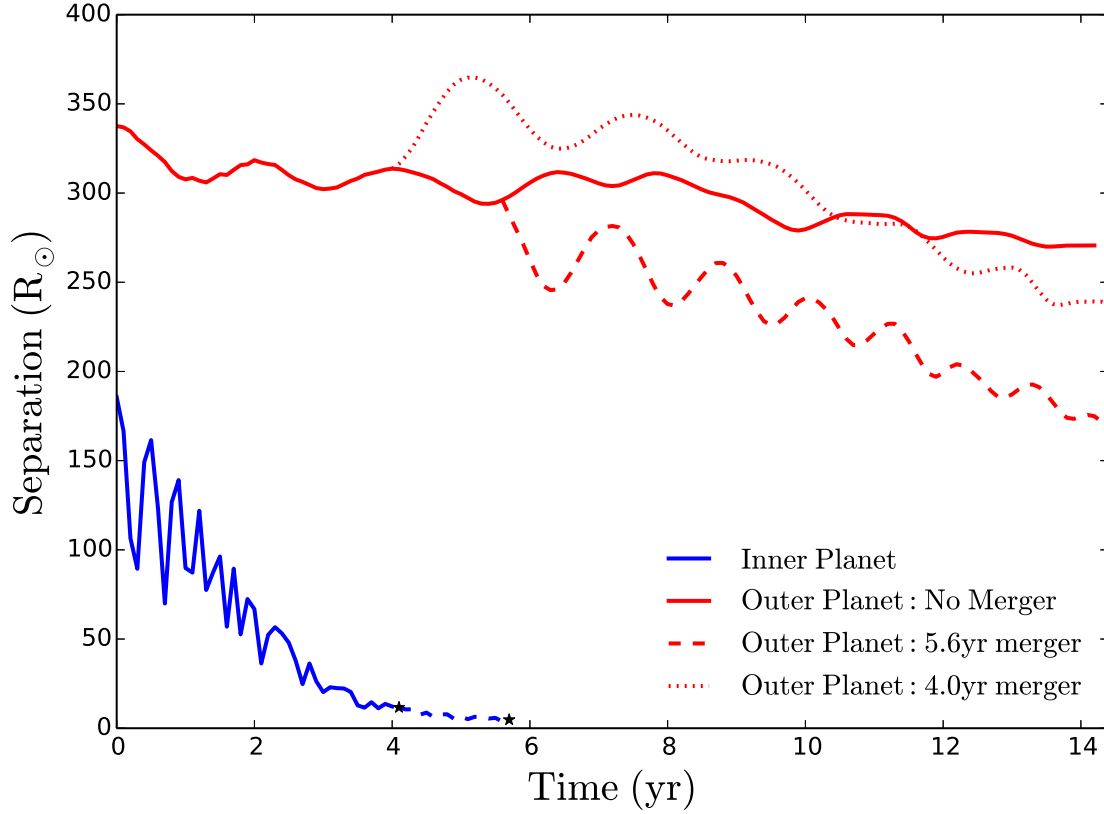(296 $R_\odot$).

Figure 3.9: The separation between the core (0.455 $M_\odot$) and the two planetary companions (10 M_J) throughout the 14.3 year simulation. The solid blue and red lines are the separations of the inner and outer planet respectively. The black stars indicate the position of the inner planet when it was removed. The dotted and dashed red lines are the separations of the outer planet after the inner planet was removed in SIM4 and SIM3 respectively.

3.3.1 Orbital evolution after the "merger"

As shown in Fig. 3.9, when the inner planet is removed, the outer planet no longer remains on a stable orbit. In both SIM3 and SIM4 the outer planet starts an in-spiral towards the primary core. In SIM4 after removing the inner planet, the outer planet temporarily moves further out before falling back to an in-spiral. The sharp turn in the orbital evolution of SIM3 after the "merger" at 5.6 years is due to the delay in the first post-merger data dump. The merger dump frequency was increased for SIM4.

The effect of the "merger" in both SIM3 and SIM4 appears to have a destabilising effect on the outer planet, causing a drastic shift in the orbital motion. For this effect to be considered "real" the delay between the removal of the planet and the deviation of the dynamics from SIM2 must be longer than the delay of information transfer. For example if the information propagation is via the gas in the envelope, then we would find a delay after removing the planet The sound speed of the gas is approximately 10 km/s (see Figure 3.3), if this was the method of information propagation then it would take in excess of half a year to reach 300$R_\odot$. From this we can conclude that either the
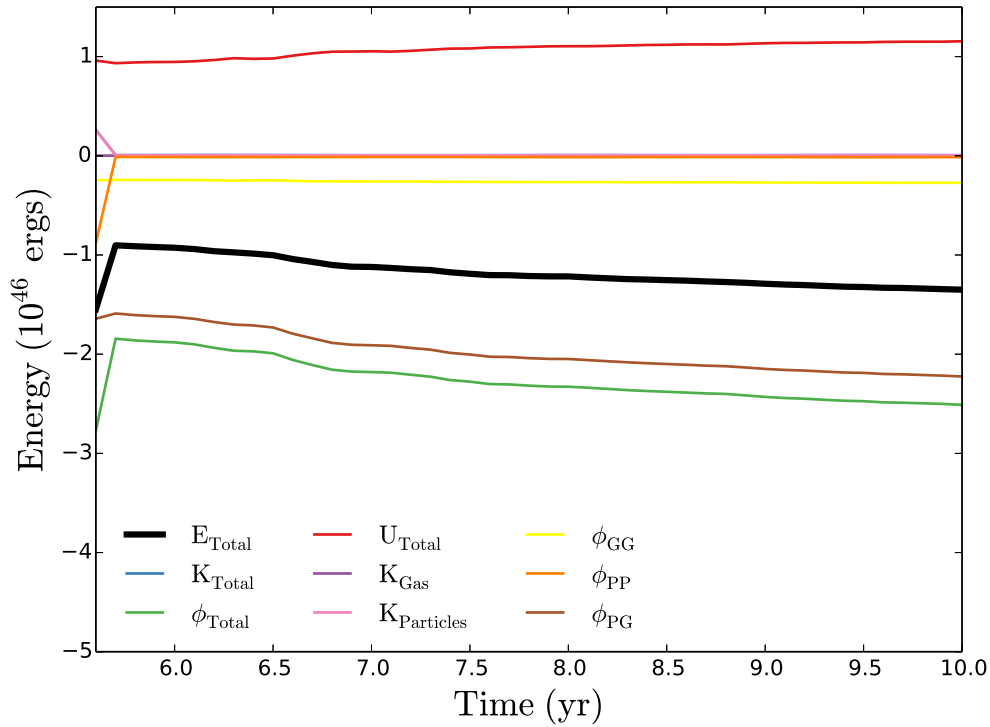
Figure 3.10: The total energy and energy components of SIM3. The labels are the same as in Fig. 3.5a

.

information is propagated by gravity, or this effect is a likely artifact.

We are cautious to believe that this effect is "real" as we are uncertain at this time of the mechanise for gravity to cause the destabilisation. This could be studied further by varying the strength of gravity in our simulations and seeing if there is a dynamical change. We are currently performing an analogous "merger" simulation in PHANTOM to add a verification step and determine that the effect is not code dependant.

To ensure that the removal of the mass was not to blame for the orbital change we carried out another simulation (SIM5 in Table 3.1). In SIM5 we replicated SIM3 with the only difference was that the mass of the "merged" inner planet was added to the mass of the cell containing the primary core. We saw no differences in the energy components between SIM3 and SIM5 over the 3.3-year test (Fig. 3.10). This suggests that not replacing the mass on the inner planet in SIM3 (and presumably SIM4) did not affect the results of the simulation. In Fig. 3.10 there is a jump in the total energy just after the restart of the simulation. Since the inner planet is deep in the potential well of the core, its total energy is negative. Removing the inner planet causes an increase in the total energy of the system.

3.4   Problems and Future Work

We mentioned in Section 3.1.1 that in SIM2 the inner particle was *erroneously* set-up on a sub-Keplerian orbit, which caused it to in-spiral faster. We also noted that from the analysis of SIM6, we do not believe that this had an effect on our conclusions. However, we should also attempt a second simulation of SIM2 with both planets correctly placed on Keplerian orbits.

We have found evidence of mass non-conservation as the inner planet gets very close to the core. This could be linked to how the AMR performed its re-griding at each time step, though logic would indicate that total energy would increase not decrease. We have also discussed how energy non-conservation worsens at the time when the inner particle penetrates the smoothing length and how the smoothing-length is poorly resolved. Finally we have not excluded an undetected bug in the energy measuring scripting, due to the difficulties encountered in keeping track of the three particles. This is the first time that mass non-conservation at this level has been seen in CE interaction ENZO.

To appropriately compare the long term stability of the outer planet's orbit in SIM2 and SIM6, we would have to run SIM6 for an additional 5 years of physical time. We expect to have some results in approximately two months from the time of writing.

Due to time constraints we only performed one SPH simulation, however this means that it is currently not possible to test the convergence of the simulation. We would require at least two more simulations with resolutions of $\sim 600,000$ and ~ 2 million particles. The latter may not be feasible.

In SIM6 we noticed the presence of a higher frequency oscillation in the orbital separation of the outer planet that matched the frequency of the in-spiral of the inner planet. A further investigation is required to determine the significance of this oscillations.

At the time of writing, we are also carrying out a PHANTOM simulation equivalent to the ENZO merger simulations SIM4 and SIM5.

4

Neutron Star Triple System

In Chapter 1 we explained that there exists an interesting pulsar known as PSR J0337+1715. This pulsar is unusual as it is a 1.438 $M_\odot$ NS that has two WD companions. We would like to understand how a system such as this one could form. Tauris & van den Heuvel (2014) proposed a CE scenario that involved a 10 $M_\odot$ entering a CE with a 1.1 $M_\odot$ main sequence companion with a second, 1.3 $M_\odot$ main sequence companion orbiting farther out.

The model presented by Tauris & van den Heuvel (2014) predicts that both the inner and outer stellar companions will in-spiral dramatically during the CE interaction. However, given that the ejection of the CE at the hand of the inner binary must have resulted in a dense outflow of gas, this raises the question, how was the outer star able to remain so far to the inner binary?

In this chapter we present the set-up and results of an ENZO simulation of a 10 $M_\odot$ RGB primary, with two companions of masses 1.1 $M_\odot$ and 1.3 $M_\odot$. This is the first simulation carried out with high resolution and modern techniques of a common envelope with a massive giant (M > 5$M_\odot$)[1] and it is the first CE simulation ever to tackle a triple system.

The star stabilisation process described in Section 4.1.2 was performed by Roberto Iaconi. The 1D stellar modelling and the 3D binary simulation was performed by the Author.

---

[1] There have been only a couple of CE simulations in the past with massive giants; a 16 and a 24 $M_\odot$ giant stars (Terman et al., 1995).

Table 4.1: Parameters for the simulations performed in this chapter. $M_1 = 9.99 M_\odot$

Sim. No.	Code	n	Resolution	τ_{run}	M_{core}	M_2	a_2/R_*	M_3	a_3/R_*
			$(R_\odot)$	(yrs)	$(M_\odot)$	$(M_\odot)$		$(M_\odot)$	
SIM7	a-grid(E)	3	5.3	0 - 4.2	2.65	1.1	1.8	1.3	7.3

4.1 Background and set-up

This simulation (SIM7 in Table 4.1) attempts to model the formation of a pulsar triple system similar to the one described by Tauris & van den Heuvel (2014). The formation method proposed by Tauris & van den Heuvel (2014) requires that both of the companion stars in-spiral, such that their periods decrease from 849 days and 4080 days (inner and outer, respectively) at the onset of the CE, to post-CE periods of 2.5 and 17.1 days.

SIM7 was performed in ENZO using a cubic box with side lengths of 25 AU (5376 $R_\odot$). The coarse grid resolution has 128 cells per side resulting in each cubic cell having a size of 42 $R_\odot$. We used four levels of refinement with a refinement factor of 2 at each level. The critical density for cell refinement is 4.18×10^{-10} g/cm^3. The smallest cell size is 5.3 $R_\odot$ on a side. We also use a smoothing length of $\epsilon = 3$ in SIM7, making the smoothing length scale 15.9 $R_\odot$.

4.1.1 Stellar structure model

Tauris & van den Heuvel (2014) (in private communication) informed us that their primary star was modelled using the stellar evolution code BEC. Their model was generated from a 10 $M_\odot$ zero-age main sequence, Milky Way metallicity ($Z = 0.0088$) star, which reached a maximum radius of 733 $R_\odot$ at the peak of the RGB.

We were unable to replicate such a star using our stellar evolution code MESA. We tested 4 different metallicities $Z = 0.001$, $Z = 0.0088$ (Milky Way value), $Z = 0.0132$ (most recent solar value) and $Z = 0.02$ (the canonical solar value) and found that increasing the metallicity increased the maximum radius of the star at the RGB (Fig. 4.1), however the maximum RGB radius was still more than 300 $R_\odot$ less than the RGB model used by Tauris & van den Heuvel (2014).

We also tried increasing the Reimer's mass-loss parameter to increase the mass loss rate. We assumed that a higher mass loss rate would cause the star to "puff up" in its outer layers. However, this yielded no difference in peak RGB radius.

Since we are unable to replicate the large star of Tauris & van den Heuvel (2014), we resigned ourselves
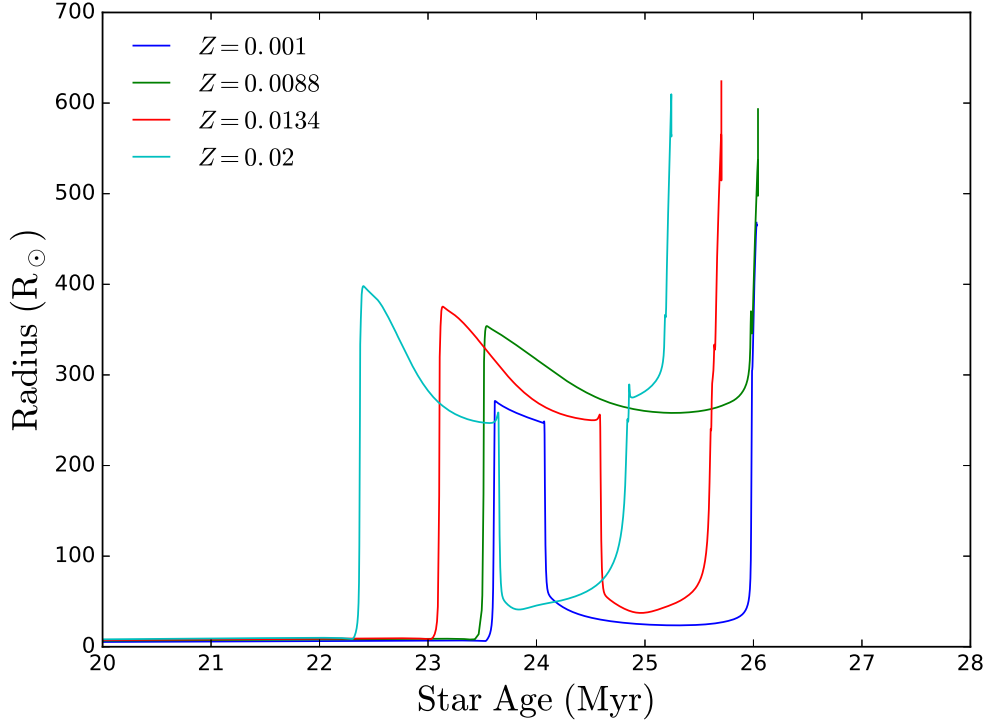
Figure 4.1: The radius evolution of 4 stars modelled in MESA with different metallicities (Z). The first peak in each curve corresponds to the peak of the RGB (the radius of interest). The higher a star's metallicity the sooner it will reach the RGB phase and the larger its radius will be.

to using a smaller star with the intention, as we explain below, to scaling down the entire system. We eventually resolved to using the $Z = 0.001$ star, with a radius 273 $R_\odot$, a total mass of 9.99 $M_\odot$ and a core mass of 3.1 $M_\odot$. The reason to use this, rather than a larger star is that, as it turned out, it was simpler to stabilise it in the 3D ENZO grid.

4.1.2 Stellar structure stabilisation in the 3D ENZO domain

Stabilising stellar structures in 3D simulations is a complex operation as explained by Passy et al. (2012a) and Iaconi et al. (2017b). Every new stellar structure seems to present some unique problems when the 1D profile is mapped into the 3D computational domain in ENZO.

Due to the difference in resolution between MESA and ENZO (see Section 3.1.1) a point particle with a mass 2.64 $M_\odot$ is added as the core. This particle has a slightly smaller mass than the core of the MESA model (3.1 $M_\odot$). The computational domain is filled with a constant low density medium (of the order of 10^{-12} g/cm^3) to help prevent the giant's outer layers from expanding. However, even with the low density background medium and a point mass core, the star is not in hydrodynamic equilibrium and expands.

We force the star into hydrodynamic equilibrium by continually damping the velocities of the gas as
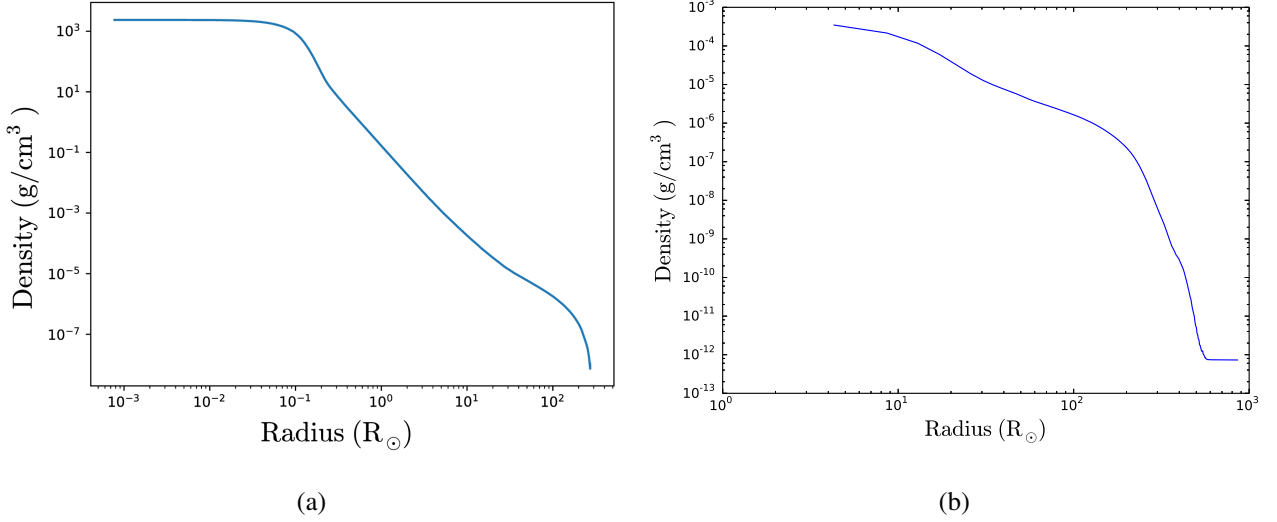
Figure 4.2: (a) Density profile of the 1D MESA model. (b) Density profile of the primary after 10.5 dynamical times of damping.

discussed in Section 3.1.1. The velocities of the gas are reduced by a factor of 3 at each time step, for approximately 10.5 dynamical times (the dynamical time of the primary is 1.43×10^7 seconds).

Larger stars are harder to stabilise than compact ones. First, the larger star has a larger range of densities than a compact star. Hence, for the same level of refinement, the internal regions of the larger star will be less resolved and thus less stable. Second, the larger star requires a longer damping phase due to instabilities that arise. The damping phase for SIM7 took 3 months of wall clock time on the supercomputer RAIJIN with 128 processors.

We chose to damp on time scales of the order of the dynamical time since the pressure gradients crossing the star act on time scale of the dynamical time. We want to equalise these pressure gradients for the star to be in hydrostatic equilibrium. Since the star is so large the dynamical time is large hence the damping time is large.

4.1.3   The orbital set-up of the two companions

The observed triple system described by Tauris & van den Heuvel (2014), has orbital separations of 811 $R_\odot$ and 2303 $R_\odot$ for the inner and outer companions, respectively ($e = 0$). Since the radius of our star is too small to undergo RLOF at these separations specified by Tauris & van den Heuvel (2014) we decided to scale down the the system. A more compact system also has the advantage that we can reduce the size of the computational domain, which yields a faster computational time.

We placed the inner companion at at a separation of 479 $R_\odot$ from the core. At this position the giant is filling its Roche lobe. We also placed the outer companion at a separation of 2000$R_\odot$ from the core.
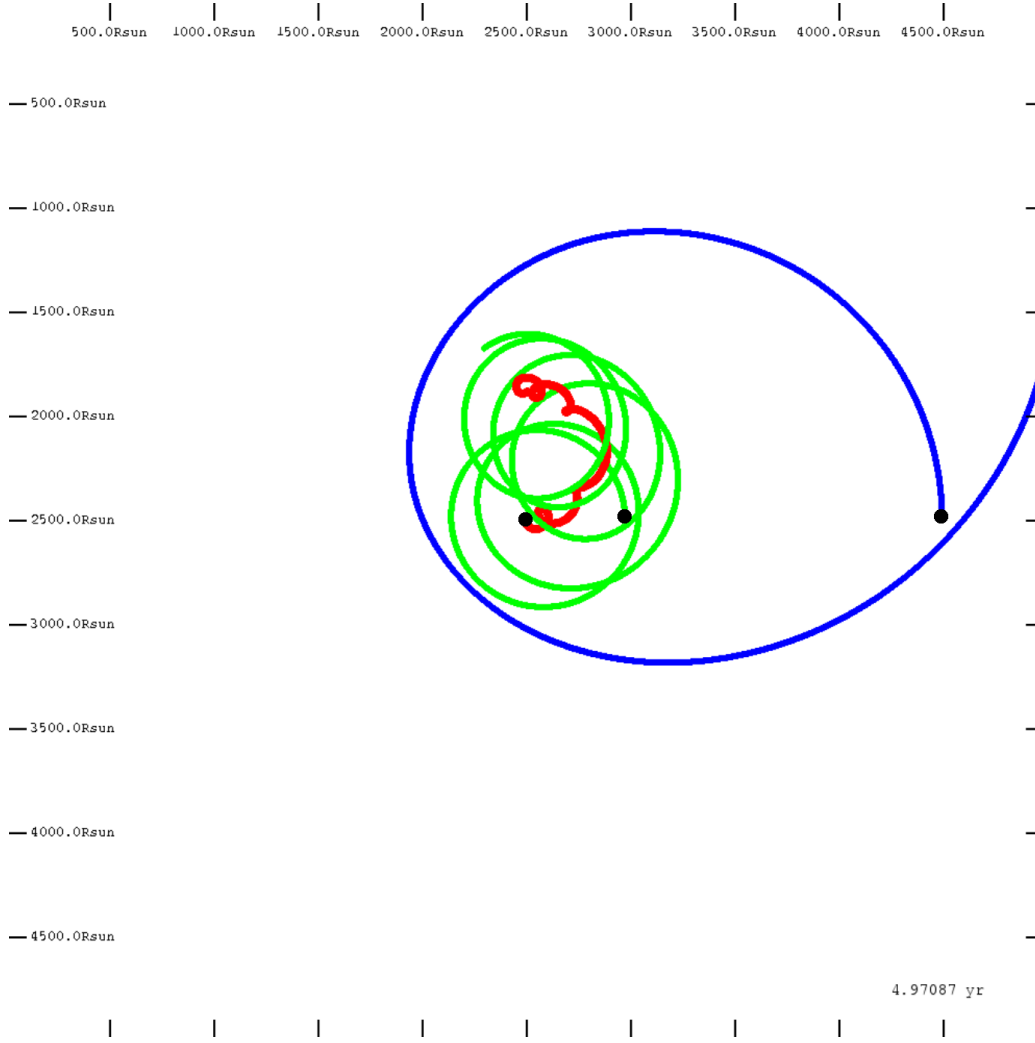
Figure 4.3: A screenshot from the N-body simulation code to test the inherent stability of the orbits in a 3-body system. The trajectories of the 9.99 $M_\odot$ primary is in red, the 1.1 $M_\odot$ inner companion is in green and the 1.3 $M_\odot$ outer companion is in blue. The black points indicate the starting positions of the three particles.

We chose the position of the outer companion such that the ratio of the outer and inner separations to approximately 4 such that the system was likely to be stable (see Mikkola et al. (2006) on the stability of triple systems).

4.1.4 N-body Simulation

Before the onset of the CE the triple system is in a stable configuration. Triple systems are able to remain stable if they have a "hierarchical structure": a short-period inner binary with the second companion in a larger distant orbit. Since we are modifying the initial set-up from that described in Tauris & van den Heuvel (2014) we would like to check if the pre-CE system is stable over a time scale longer than the CE simulation time. If not, we may not be able to discern between the effect of the CE and the effect of the natural orbital instability.

In order to check the stability of the new configuration we wrote a 3D N-body simulation visualisation
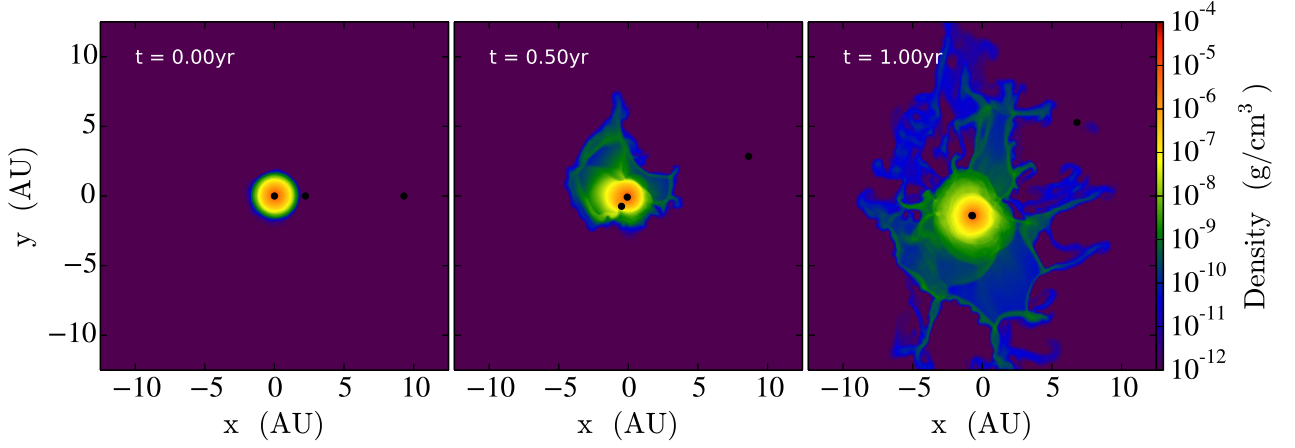
Figure 4.4: Density slices along the orbital plane after from left to right 0, 0.5 and 1 years from the beginning of SIM7. The core of the primary and the stellar companions are represented as black dots. The size of the points is not indicative of any physical property of the masses.

code. This code (which is available on github²) iteratively solves Newton's second law ($\mathbf{F} = -\nabla U$) using a fourth-order Runge-Kutta method (Chapra, 2006). The code then displays the positions of the particles visually.

In the N-body code we placed 10 $M_\odot$ particle at the centre of a $5000 \times 5000 \times 5000$ $R_\odot$ display with two particles with masses 1.1 $M_\odot$ and a 1.3 $M_\odot$ placed with separations of 479 $R_\odot$ and 2000 $R_\odot$ from the central particle respectively. The particles were placed in Keplerian orbits around the centre of mass with an initial velocity in the y direction of -6.6 km/s, $+59.6$ km/s, $+27.5$ km/s for the primary, innermost and outermost companion, respectively. We calculated the velocities by first considering a Keplerian orbit of M_1 and M_2 and then of $M_1 + M_2$ and M_3 (M_1, M_2, M_3 are the star, the inner companion and the outer companion, respectively). This set-up aims to mimic the pre-CE system of our simulation. Fig. 4.3 displays a screenshot of the simulation.

In the simulation the inner companion maintains a circular orbit around the central star with an orbital separation of 500 ± 50 $R_\odot$ over 5 years. The outer companion only completes one full orbit in 5 years before leaving the simulation domain. However, it remains in a close orbit ($E_{\text{Total}} < 0$) for the 8 years of the simulation. We therefore surmise that so long as the CE simulation runs for a physical time that is smaller than 8 years, any effects such as in-spiral or ejection of the outer companion would not be due to inherent orbital instability, but rather the CE interaction itself.
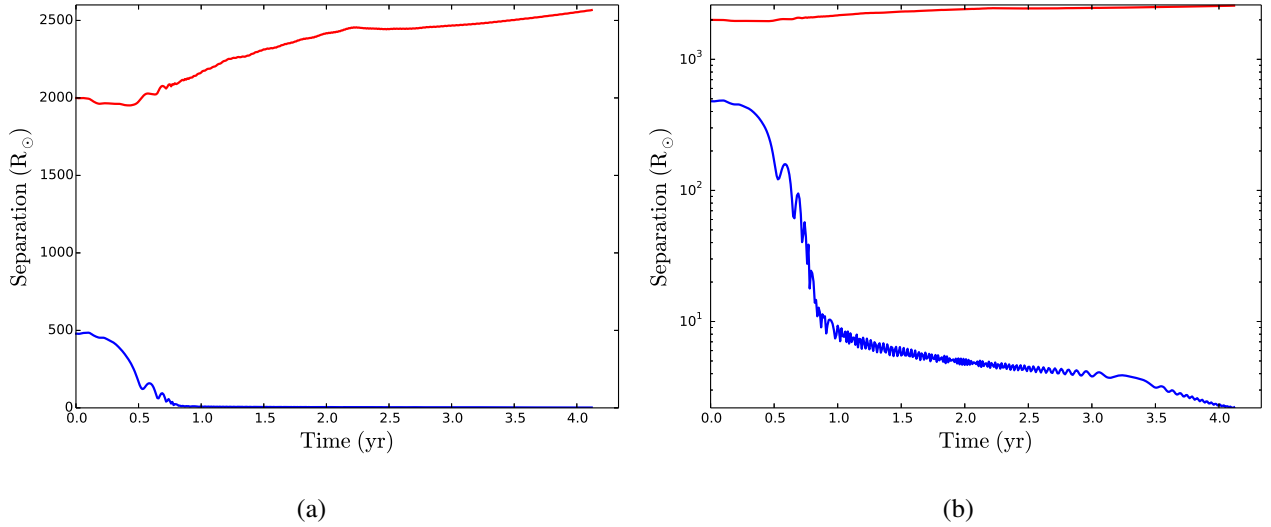
Figure 4.5: (a) The separations between the primary core and the two stellar companions. The outer companion is in red and the inner companion is in blue. (b) The same as left but with a log scaled *y* axis.

4.2   Results and discussion

Due to the size of the computational domain in SIM7 and the 4 levels of refinement, the computational time to run the simulation is very long. Combining the damping process and the simulation time, SIM7 required 7 months to run.

Fig. 4.5 shows the separations of the two stellar companions in SIM7. Since we placed the inner companion at a radius such that the primary star just fills its Roche lobe, the inner companion is rapidly engulfed by the envelope and in-spirals towards the core. The velocity components of the gas surrounding the companions are shown in Fig. 4.6. The relative velocity between the inner companion and its surrounding gas is large (peaking at ~ 175 km/s at 1 year) causing a strong gravitational drag which leads to its in-spiral. The inner companion penetrates the smoothing length just before 1 year after which time its behaviour cannot be considered reliable.

On the other hand, the outer companion does not in-spiral as envisaged by Tauris & van den Heuvel (2014). Its separation increases during the in-spiral (it increases by 25% over the first 4 years). The separation continues to increase even later, when the envelope displaced by the inner companion's in-spiral reaches the outer companion. The relative velocity between the outer companion and the gas surrounding it is very low Fig. 4.6 indicating that the gas is co-rotating. This implies that the gravitational drag that would typically cause an in-spiral in this case is small. We estimate that the time scale to establish co-rotation between the secondary and the envelope is approximately 1.2 years. The radial velocity component of the surrounding gas (solid blue line in Fig. 4.6) oscillates above and

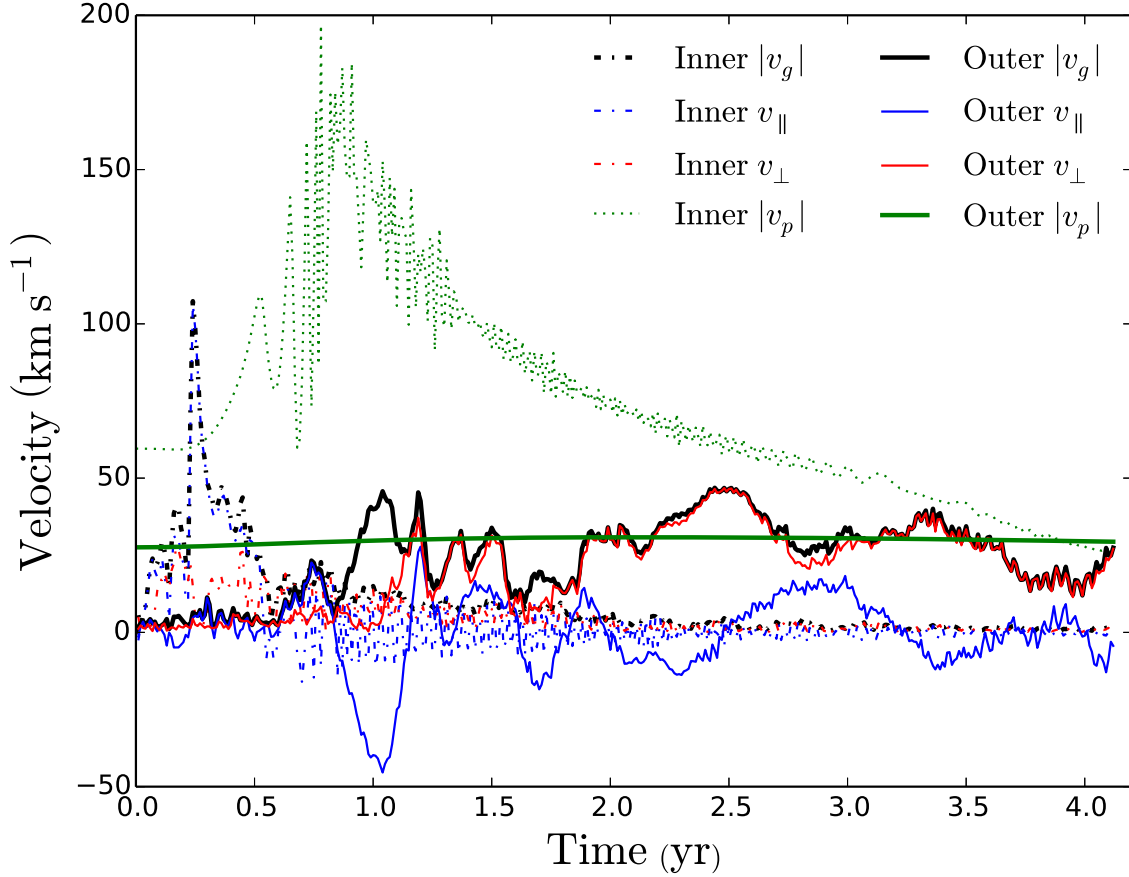---

[2]https://github.com/abatten/gravitational-nbody-visualisation

Figure 4.6: The velocity components of the gas around the two companions in SIM7. "Outer" and "Inner" refer to the outermost and innermost companion, respectively. $|v_g|$ is the average velocity magnitude of the gas at the position of the the companion, $v_{||}$ is radial component of $|v_g|$, $v_\perp$ is the component of $|v_g|$ perpendicular $v_{||}$, $|v_p|$ is the velocity magnitude of the companion with respect to the grid. $v_{||}$ represents the outwards moving gas and $v_\perp$ represents the gas moving in the same direction as the companion.

below zero, suggesting that there is no net outflow of gas, and thereby no net outwards drag (as was instead the case for the outer companion in SIM2, Chapter 3).

The increase in separation of the outer companion (from $2000\,R_\odot$ to $2500\,R_\odot$) over 4.2 years is greater than what we observe in the 3-body case over the same time ($2000\,R_\odot$ to 2130). In the 4 years of the hydrodynamic code, the outer companion has only completed half an orbit, whereas in the N-body simulation it completed a whole orbit.

Similarly to what we proposed for the planets in Chapter 3, a radial outflow could push the outer companion farther outwards. However, SIM7 does not display a clear positive outflow at the location of the outer companion (blue solid curve in Fig. 4.6), but rather we observe a complex behaviour.

Upon checking for mass conservation, we find that $0.08\,M_\odot$ has been lost from the simulation in the first 2.7 years (Fig. 4.7a). Almost all of this mass loss is due to outflow from the simulation boundary:
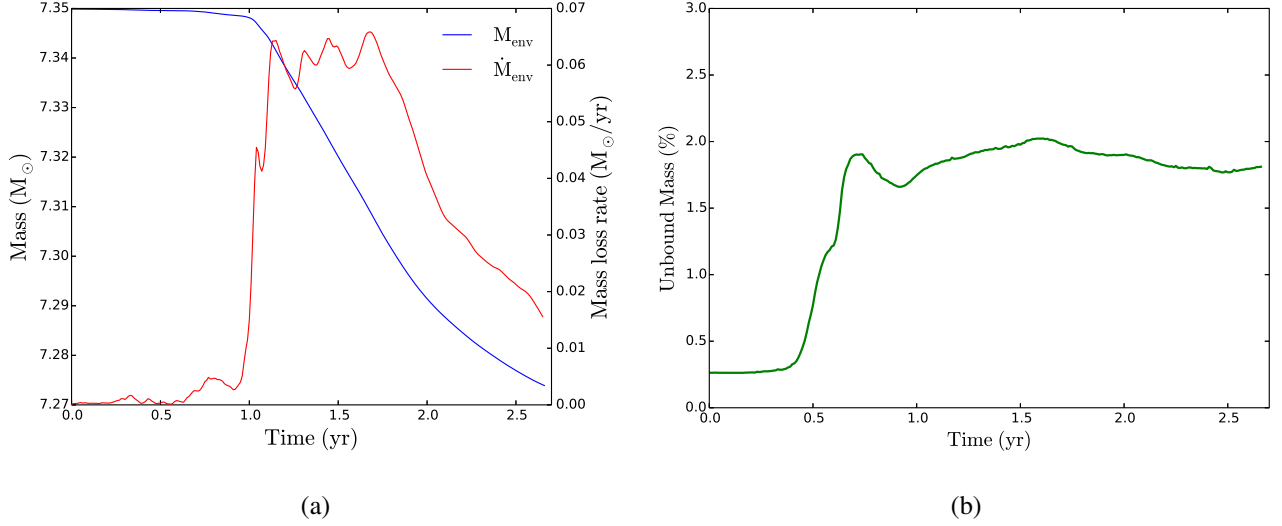
(a)   (b)

Figure 4.7: (a) The total envelope mass (M_{env}) and envelope mass loss rate ($\dot{M}_{env}$) of the envelope for SIM7. (b) The unbound mass percentage (i.e., $E_{Total} > 0$) in SIM7.

we estimate that more than 98% is due to outflow, with $\sim 2\%$ due to mass non-conservation as was the case in the planet simulation in Chapter 3.

Very little of the envelope becomes unbound ($\sim 2\%$). This is what we expect from simulations that do not include recombination as an additional source of energy (Passy et al., 2012a; Iaconi et al., 2017b). Recombination energy has been shown to enable some simulations to eject the envelope of low mass stars (Nandez & Ivanova, 2016). Our own implementation of recombination energy in PHANTOM (Reichardt et al. in preparation) confirms this, but also raises the question of how much of the recombination energy should be available to unbind the envelope and how much would leave as radiation on short time-scales. Recombination energy would likely increase the mass of the outflow something that may promote further in-spiral of the outer companion or may contribute to pushing it farther out.

4.3   Problems, solutions and future work

There is a lot of scope for CE simulations with massive primaries ($M > 10$ M$_\odot$), which in the end result in NSs. The formation path to double NSs, which may merge with the emission of detectable gravitational waves (Kasliwal et al., 2017), includes multiple CE phases. Modelling these phases are important for population synthesis studies (Belczyński & Kalogera, 2001), since they assume knowledge of the CE interaction. Carrying out a simpler, two-body simulation with one companion would be advisable to catalogue issues pertaining to CE simulations in this new, massive regime. This said, it is very likely that a simulation with only one companion would be similar to this simulation:

the addition of an outer companion likely does not affect the inner companion in-spiral and ejection properties of the envelope.

The addition of recombination energy in the simulation would allow us to study the behaviour of a more massive outflow on the outer companion. We could have attempted to stabilise the primary in the SPH code. This would reduce the computational requirements due to the large ENZO computational domain and there would be no danger of the outer star leaving the box. As recombination energy is now implemented in PHANTOM, we could determine whether this addition can eject the envelope of 10 M$_\odot$ stars. This may change the dynamics of the interaction.

At the time of writing, we are running another simulation with 5 levels of refinement. This simulation better samples the strong gradients around the stellar core and companions. However, due to the increased resolution, the computational time for the simulation increased tremendously and the simulation has not reached one year of physical time at the time of writing.

5

Conclusions and future work

In SIM2 although the inner planet was rapidly engulfed into the CE, we found that the outer planet maintains an orbital separation of approximately 300 $R_\odot$, with a very gradual decay over 14 years. We ruled out energy and angular momentum non-conservation as the cause of this result using an SPH simulation which exhibited similar properties while conserving energy almost perfectly. We also are reasonably sure that the simulation resolution did not play a role in the orbital stability, though some testing would be advisable. We may have found evidence for resonances between the inner and outer planet orbits using the SPH simulation, something that warrants further study. We conclude, preliminarily, that the orbital stability of the outer planet is due, at least in part, to the outflow of gas promoted by the in-spiral of the inner companion.

When the innermost planet is removed (it merges with the core) we found some evidence that the outer planet may in-spiral more readily. We are currently carrying our an SPH "merger" simulation in PHANTOM to verify the destabilisation effect we see in ENZO is not code-dependant.

Our 10 $M_\odot$ RGB star simulation with two, solar-mass companions results in the outer companion moving out, rather than in, as envision instead by Tauris & van den Heuvel (2014) in the formation

of the triple pulsar PSRJ0337+1715. In this case we cannot say for sure that the gas outflow is responsible. This simulation, a first of its kind, needs additional testing to be fully interpreted.

Our original hypothesis Chapter 1, was that the action of a tertiary companion (inner or outer) may impact the behaviour of the secondary companion in the context of a common envelope interaction, in that it would leave at least one companion at an intermediate separation. What we observed in our simulations, however, would point to outer companions moving outwards, farther than they had started and would therefore be found at larger separation than the original radius of the giant, not smaller. At best, the outer companion would stay at a similar separation.

This conclusion is reasonably firm for the planet case, where an outward flow would easily generate an outward force. On the other hand this was less clear in the case of the massive triple simulation. We also should add the caveat that the inclusion of recombination energy by adopting a non-ideal gas equation of state (as done by Nandez & Ivanova (2016)) would promote a more massive outflow, which may result in some in-spiral because of the larger mass bathing the outer companion, though it could also promote a stronger outer force because of the faster velocities. SPH simulations with recombination energy, equivalent to our SIM8 should therefore be carried out to test the effect of recombination energy.

A

Gravitational 3D nbody Code

I wrote a gravitational N-body simulation code in python can displays the interaction visually. The code solves Newton's second law using a fourth order Runge-Kutta method. The code is available on Github (github/abatten/gravitational-nbody-visualisation).

A.1 Example

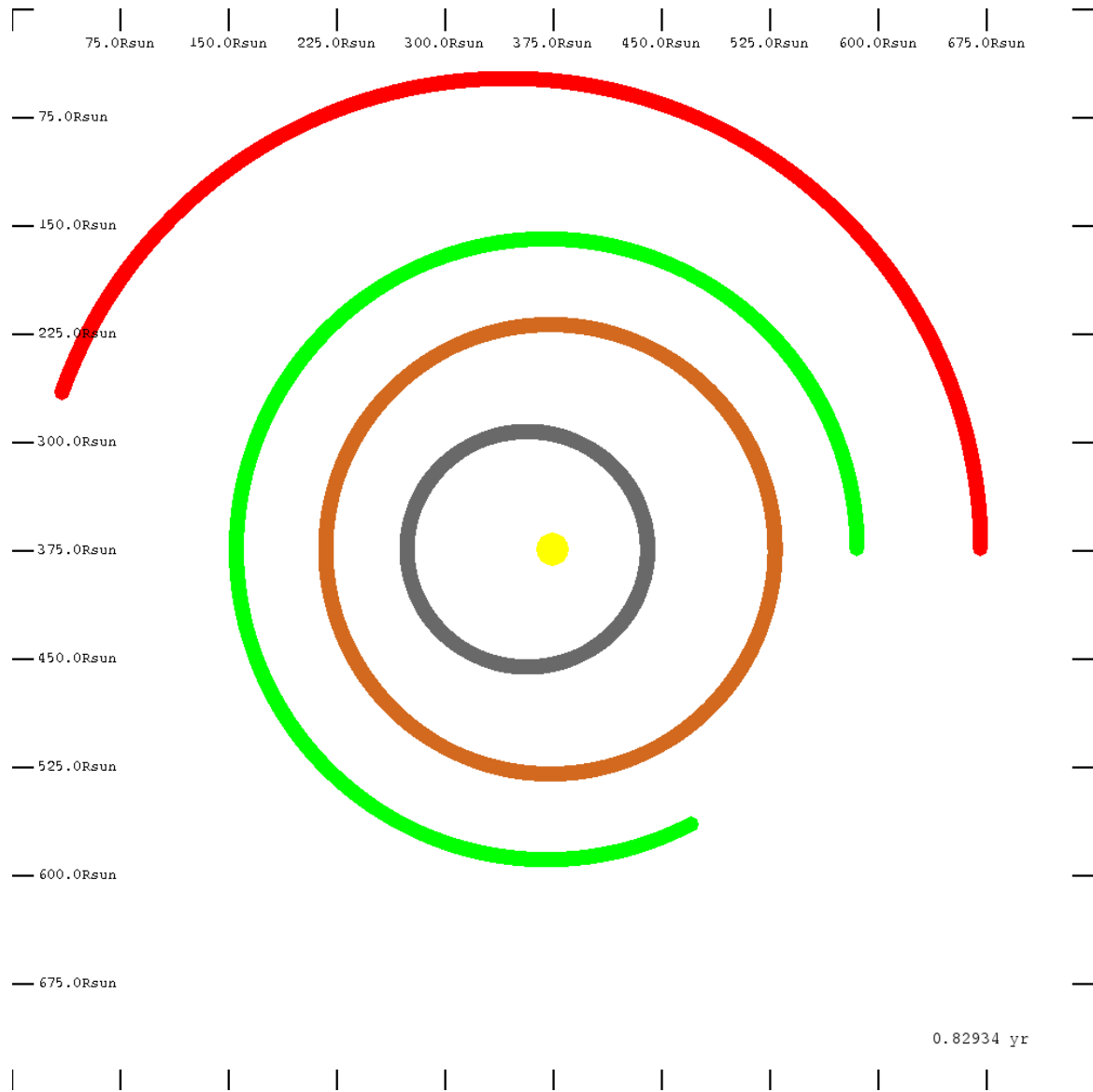An example of the output of the N-body code using our own solar system as a model.

Figure A.1: The trajectories of the 4 inner planets of our solar system as modelled using the gravitational N-body code. The yellow circle is the sun. The grey path is Mercury, orange is Venus, green is Earth and red is Mars.

A.2   Code

A.2.1   Runge-Kutta Function

```python
def rk4(particle, particleList, dt):
    """
    Returns position and velocity of a particle after a timestep.
    ---- Parameters ----
    particle (Particle) : The particle to update its pos and vel.
    particleList (List) : The list of all gravitating particles.
    dt (float) : The time step to increase by.
    ---- Returns ----
    new_pos (numpy.array) : New position vector of the particle.
    new_vel (numpy.array) : New velocity vector of the particle.
    """
    #  Current Positions, Velocity and Acceleration
    kv1 = particle.vel
    kp1 = particle.pos
    ka1 = particle.acceleration(kp1, particleList)
    #  Step 2
    kv2 = kv1 + 0.5 * dt * ka1
    kp2 = kp1 + 0.5 * dt * kv2
    ka2 = particle.acceleration(kp2, particleList)
    #  Step 3
    kv3 = kv1 + 0.5 * dt * ka2
    kp3 = kp1 + 0.5 * dt * kv3
    ka3 = particle.acceleration(kp3, particleList)
    #  Step 4
    kv4 = kv1 +  dt * ka3
    kp4 = kp1 +  dt * kv4
    ka4 = particle.acceleration(kp3, particleList)
    #  Final positions and velocities
    new_vel = kv1 + (1./6.) * dt * (ka1 + 2 * (ka2 + ka3) + ka4)
    new_pos = kp1 + (1./6.) * dt * (kv1 + 2 * (kv2 + kv3) + kv4)
    return new_pos, new_vel
```

A.2.2   Particle Class

The RK4 function depends on the class 'Particle' as defined below.

```python
class Particle:
    """

    Class to represent point masses.
    ---- Parameters ----
    win (pygame.display) : Window to display the particle
    pos (list 3D) : Particle coordinates [Unit: Rsun].
    vel (list 3D) : Velocity vector of the particle [Unit: km/s].
    mas (float) : Mass of the particle [Unit: Msun].
    rad (int) : Radius of the particle displayed [Unit: pixels].
    col (RGB tuple) : Colour of the particle
    """
    def __init__(self, win, pos, vel, mass=1, rad=4, col=(0,0,0)):
        self.pos = np.array([x * C.XRSUN for x in pos]) # Rsun -> m
        self.vel = np.array([v * C.XKM for v in vel])   # km/s -> m
        self.mas = mass * C.XMSUN   # Msun -> kg
        self.rad = rad
        self.col = col
    def __repr__(self):
        return ('Pos:{x} Vel:{v} Mass:{m} Rad:{r} Col:{c}'.format(
                x=self.pos, v=self.vel, m=self.mas,
                r=self.rad, c=self.col))
    def draw(self, win, SCALE):
        """

        Draws the particle in its initial position.
        ---- Parameters ----
        win (pygame.display) : Window to display the particle
        """

        pyg.draw.circle(win, self.col,
                        (int(self.pos[0]/C.XRSUN*SCALE),
                        int(self.pos[1]/C.XRSUN*SCALE)),
                        int(self.rad*SCALE) + 2 , 0)
    def dist_to(self, other):
        """ Find the distance between a particle and itself. """
```

```python
        dist = np.linalg.norm(self.pos - other.pos)
        return dist


    def acceleration(self, position, particleList):
        """
        Finds the particles acceleration due to other particles.
        ---- Parameters ----
        position (numpy.array) : Position to find the grav accel
        particle_list (list) : List of all gravitating particles
        ---- Returns ----
        a (numpy.array) : The acceleration components of particle
        """
        a = np.zeros(3)
        for p1 in particleList:
            if p1 is not self:
                delta = p1.pos - position
                dist = self.dist_to(p1)
                dsquared = dist**2.0
                #  C.XG is the Gravitational Constant
                Force = C.XG * self.mas * p1.mas / dsquared
                a += (Force / self.mas) * (delta / dist)
        return a
```

B

Analysis Code

In this appendix I report an original Python analysis code which was specifically written to analyse the outputs of the ENZO simulations. We present only one script but 13 other scripts were also written for the data analysis which can be found on Github (https://github.com/abatten/common-envelope-analysis).

B.1 Companion Separation Script

```python
from __future__ import absolute_import, division, print_function
import yt.mods as yt
import numpy as np
import sys
import ConfigParser
import cemodules.cefunctions as cef



def read_inlist(ipath):
    inlist_name = ipath.split('/')[-1]
    config = ConfigParser.ConfigParser()
    config.readfp(open(inlist_name, 'r'))
```

```python
    # Read in the config file
    root_dir = config.get("Common", "root_dir")
    exclude_dir = config.get("Common", "exclude_dir")
    plot_dir = config.get("Common", "plot_dir")
    initial_path = config.getint("Common", "initial_path")
    final_plus_one = config.getint("Common", "final_plus_one")
    output_file_name = config.get("Separation", "output_file_name")
    particle_number = config.getint("Common", "particle_number")

    return (root_dir, exclude_dir, plot_dir, initial_path,
            final_path_plus_one, output_file_name, particle_number)

def open_file(file_name, num_particles):
    output_file = open(file_name, 'w')
    header = "Time(yr), Cycle(#)"

    # Create header based on the number of particles
    header_dict = {}
    for i in range(num_particles-1):
        dict[str(i)] = "separation_%s_%s_(cm)" % ("Companion", i)
        header = ", ".join([header, dict[str(i)]])

    # Write the first line of information in the file
    output_file.write(header + "\n")
    return output_file

def separations(directory, output_file, particle_number):
    pf = yt.load(directory)

    #  Gets the length, time and mass units used in the simulation
    lu = pf.parameters['LengthUnits']
    tu = pf.parameters['TimeUnits']
    current_cycle = pf.parameters['InitialCycleNumber']
    current_time = pf.current_time

    #  Adds the whole data as an object.
```

```python
ce = pf.h.all_data()


yr = 365.25 * 24 * 60 * 60
current_time = pf.current_time / yr


# Find the corresponding to the primary index.
# I.e. the particle with the largest mass
particle_masses = ce["ParticleMassMsun"]
prim_mass = np.max(particle_masses)
for i in range(len(particle_masses)):
    if particle_masses[i] == prim_mass:
        prim_index = i
        break
    else:
        pass
# Coordinates of the Primary Star
prim_coords = [ce['particle_position_x'][prim_index] * lu,
               ce['particle_position_y'][prim_index] * lu,
               ce['particle_position_z'][prim_index] * lu]


sep = {}
for i in range(particle_number):
    #  Get particle index list to track individual particles
    pdex = ce['particle_index']

    if i != prim_index:
        comp_coords = [ce['particle_position_x'][i] * lu,
                       ce['particle_position_y'][i] * lu,
                       ce['particle_position_z'][i] * lu]

        separation = cef.distance(prim_coords, comp_coords)
        sep[pdex[i]] = separation

row = str(current_time * tu) + " " + str(current_cycle)


for i in range(len(sep.items())):
```

```python
        row = " ".join([row, str(sep.items()[i][1])])


    output_file.write(row + "\n")


if __name__ == "__main__":
    yt.mylog.disabled = True


    (root_dir, exclude_dir,
     plot_dir, initial_path,
     final_path_plus_one, output_file_name,
     particle_number) = read_inlist(sys.argv[1])


    # Sort the root directory
    root_dir_list = cef.root_sort(root_dir, exclude=exclude_dir)


    # Set output file name and open it to write
    output_file_name = plot_dir + output_file_name
    output_file = open_file(output_file_name, particle_number)


    for index in range(initial_path, final_plus_one):
separations(root_dir_list[index], output_file, particle_number)
```

References

Abbott, B. P., Abbott, R., Abbott, T. D., et al. 2016a, Physical Review Letters, 116, 241103

—. 2016b, Physical Review Letters, 116, 061102

—. 2017a, Physical Review Letters, 118, 221101

—. 2017b, Physical Review Letters, 119, 141101

—. 2017c, Physical Review Letters, 119, 161101

Akashi, M., & Soker, N. 2017, Monthly Notices of the Royal Astronomical Society, 1

Belczyński, K., & Kalogera, V. 2001, The Astrophysical Journal, 550, L183

Beuermann, K., Hessman, F. V., Dreizler, S., et al. 2010, Astronomy and Astrophysics, 521, L60

Blagorodnova, N., Kotak, R., Polshaw, J., et al. 2017, The Astrophysical Journal, 834, 1

Bodenheimer, P. H., Lin, D. N. C., & Mardling, R. A. 2001, The Astrophysical Journal, 548, 466

Bond, H. E., Henden, A., Levay, Z. G., et al. 2003, Nature, 422, 405

Bondi, H. 1951, Monthly Notices of the Royal Astronomical Society, 112, 195

Bryan, G. L., Norman, M. L., O'Shea, B. W., et al. 2014, The Astrophysical Journal Supplement Series, 211, 19

Chapra, S. C. 2006, Applied Numerical Methods with MATLAB for Engineers and Scientists (McGraw-Hill Science/Engineering/Math)

Charpinet, S., Fontaine, G., Brassard, P., et al. 2011, Nature, 480, 496

Claeys, J. S. W., Pols, O. R., Izzard, R. G., Vink, J., & Verbunt, F. W. M. 2014, Astronomy and Astrophysics, 83, 1

de Kool, M. 1990, The Astrophysical Journal, 358, 189

De Marco, O. 2009, Publications of the Astronomical Society of the Pacific, 121, 316

De Marco, O., & Izzard, R. G. 2017, Publications of the Astronomical Society of Australia, 34, e001

De Marco, O., Passy, J.-c., Moe, M., et al. 2011, Monthly Notices of the Royal Astronomical Society, 2292, 2277

Dewi, J., & Tauris, T. 2000, Astronomy & Astrophysics, 360, 1043

Duchêne, G., & Kraus, A. 2013, Annual Review of Astronomy and Astrophysics, arXiv:1303.3028

Eggleton, P. P. 1983, The Astrophysical Journal, 268, 368

Fabrycky, D. C., & Tremaine, S. 2007, The Astrophysical Journal, 669, 1298

Fuhrmann, K., & Chini, R. 2012, The Astrophysical Journal Supplement Series, 203, 20

—. 2015, The Astrophysical Journal Supplement Series, 809, 19

Garcia-Segura, G., Langer, N., Rożyczka, M., & Franco, J. 1999, The Astrophysical Journal, 517, 767

García-Segura, G., Villaver, E., Langer, N., & Manchado, A. 2014, The Astronomical Journal, 783

Hillebrandt, W., & Niemeyer, J. C. 2000, Annual Review of Astronomy and Astrophysics, 38, 191

Hopkins, A. M., & Beacom, J. F. 2006, The Astrophysical Journal, 651, 142

Iaconi, R., Marco, O. D., Passy, J.-c., & Staff, J. 2017a, Monthly Notices of the Royal Astronomical Society, 16, 1

Iaconi, R., Reichardt, T., Staff, J., et al. 2017b, Monthly Notices of the Royal Astronomical Society, 464, 4028

Iben, I. J., & Livio, M. 1993, Publications of the Astronomical Society of the Pacific, 105, 1373

Ivanova, N., & Nandez, J. L. 2016, Monthly Notices of the Royal Astronomical Society, 462, 362

Ivanova, N., Justham, S., Chen, X., et al. 2013, Astronomy and Astrophysics Review, 21, arXiv:1209.4302

Jones, D., & Boffin, H. M. J. 2017, Nature Astronomy, 1, 1

Kasliwal, M. M., Nakar, E., Singer, L. P., et al. 2017, arXiv:1710.05436

Kouwenhoven, M. B. N., Brown, A. G. A., Zinnecker, H., Kaper, L., & Zwart, S. F. P. 2005, Astronomy and Astrophysics, v.430, p.137-154 (2005), 430, 137

Kozai, Y. 1962, The Astronomical Journal, 67, 591

Kuruwita, R. L., Staff, J., & De Marco, O. 2016, Monthly Notices of the Royal Astronomical Society, 461, 486

Livio, M., & Pringle, J. E. 2011, The Astrophysical Journal Letters, 740, 4

Macleod, M., Antoni, A., Murguia-berthier, A., Macias, P., & Ramirez-ruiz, E. 2017a, The Astrophysical Journal, 838, 56

Macleod, M., Macias, P., Ramirez-ruiz, E., et al. 2017b, The Astrophysical Journal, 835, 1

Macleod, M., & Ramirez-Ruiz, E. 2015, The Astrophysical Journal, 803, 41

Marsh, T. R., Parsons, S. G., Bours, M. C. P., et al. 2013, Monthly Notices of the Royal Astronomical Society, 437, 475

Mikkola, S., Innanen, K., Wiegert, P., Connors, M., & Brasser, R. 2006, Monthly Notices of the Royal Astronomical Society, 369, 15

Mustill, A. J., Marshal, J. P., Villaver, E., et al. 2013, Monthly Notices of the Royal Astronomical Society, 436, 2515

Nandez, J. L., & Ivanova, N. 2016, Monthly Notices of the Royal Astronomical Society, 462, 362

Nandez, J. L. A., Ivanova, N., & Lombardi, J. C. 2015, Monthly Notices of the Royal Astronomical Society: Letters, 450, L39

Nordhaus, J., Blackman, E. G., & Frank, A. 2007, Monthly Notices of the Royal Astronomical Society, 376, 599

Ohlmann, S. T., Röpke, F. K., Pakmor, R., & Springel, V. 2016a, The Astrophysical Journal, 816, L9

Ohlmann, S. T., Röpke, F. K., Pakmor, R., Springel, V., & Müller, E. 2016b, Monthly Notices of the Royal Astronomical Society: Letters, 462, L121

O'Shea, B. W., Bryan, G., Bordner, J., et al. 2004, arXiv:astro-ph/0403044

Ostriker, E. C. 1999, The Astrophysical Journal, 513, 252

Paczynski, B. 1976, in IAU Symp. 73:P Structure and Evolution of Close Binary Systems, Vol. 73, 75

Parsons, S. G., Marsh, T. R., Copperwheat, C. M., et al. 2010, Monthly Notices of the Royal Astronomical Society, 402, 2591

Passy, J.-C., & Bryan, G. L. 2014, The Astrophysical Journal Supplement Series, 215, 8

Passy, J.-C., Mac Low, M.-M., & De Marco, O. 2012a, The Astrophysical Journal, 759, L30

Passy, J.-C., De Marco, O., Fryer, C. L., et al. 2012b, The Astrophysical Journal, 744, 52

Paxton, B., Bildsten, L., Dotter, A., et al. 2011, The Astrophysical Journal Supplement Series, 192, 35

Paxton, B., Cantiello, M., Arras, P., et al. 2013, The Astrophysical Journal Supplement Series, 208, 43

Price, D. J., Wurster, J., Nixon, C., et al. 2017, Publications of the Astronomical Society of Australia (PASA), arXiv:1706.01246

Raghavan, D., McAlister, H. A., Henry, T. J., et al. 2010, The Astrophysical Journal Supplement Series, 190, 1

Ransom, S. M., Stairs, I. H., Archibald, A. M., et al. 2014, Nature, 505, 520

Rappaport, S., Deck, K., Levine, A., et al. 2013, The Astrophysical Journal, 768, 33

Rasio, F. A., & Livio, M. 1996, Astrophysical Journal, 471, 366

Ricker, P. M., & Taam, R. E. 2008, The Astrophysical Journal, 672, L41

—. 2012, The Astrophysical Journal, 746, 74

Riess, A. G., Filippenko, A. V., Challis, P., et al. 1998, The Astronomical Journal, 116, 1009

Ruffert, M. 1993, Astronomy and Astrophysics, 288, 141

Sana, H., de Mink, S. E., de Koter, A., et al. 2012, Science, 337, 444

Sandquist, E., Taam, R. E., Lin, D. N. C., & Burkert, A. 1998, The Astrophysical Journal, 506, 11

Shu, F. H. 1982, The Physical Universe (University Science Books)

Smith, N., Andrews, J. E., Dyk, S. D. V., et al. 2016, Monthly Notices of the Royal Astronomical Society, 458, 950

Soker, N. 2006, Publications of the Astronomical Society of the Pacific, 118, 260

Staff, J. E., De Marco, O., Macdonald, D., et al. 2016a, Monthly Notices of the Royal Astronomical Society, 455, 3511

Staff, J. E., Marco, O. D., Wood, P., Galaviz, P., & Passy, J.-c. 2016b, Monthly Notices of the Royal Astronomical Society, 458, 832

Taam, R. E., & Sandquist, E. L. 2000, Annual Review of Astronomy & Astrophysics, 38, 113

Tauris, T. M., & van den Heuvel, E. P. J. 2014, The Astrophysical Journal Letters, 781, L13

Terman, J. L., Taam, R. E., & Hernquist, L. 1995, ApJ, 445, 367

Thorne, K. S., & Żytkow, A. N. 1977, The Astrophysical Journal, 212, 832

Tocknell, J., De Marco, O., & Wardle, M. 2014, Monthly Notices of the Royal Astronomical Society, 439, 2014

Tokovinin, A., Thomas, S., Sterzik, M., & Udry, S. 2006, Astronomy & Astrophysics, 450, 681

Toonen, S., Claeys, J. S. W., Mennekens, N., & Ruiter, A. J. 2014, Astronomy and Astrophysics, 14

Turk, M. J., Smith, B. D., Oishi, J. S., et al. 2011, The Astrophysical Journal Supplement Series, 192, 9

Tylenda, R., Hajduk, M., Kami, T., et al. 2011, Astronomy & Astrophysics, 114, 1

Udry, S., & Santos, N. C. 2007, Annual Review of Astronomy & Astrophysics, 45, 397

van den Heuvel, E. P. J. 1976, in Structure and Evolution of Close Binary Systems, Vol. 73, 35

Van Winckel, H. 2003, Annual Review of Astronomy and Astrophysics, 41, 391

Van Winckel, H., Lloyd Evans, T., Briquet, M., et al. 2009, Astronomy and Astrophysics, 505, 1221

Webbink, R. F. 1984, The Astrophysical Journal, 277, 355

Webbink, R. F. 2008, in Astrophysics and Space Science Library, ed. E. F. Milone, D. A. Leahy, & D. W. Hobill